© 2021. Published by The Company of Biologists Ltd | Development (2021) 148, dev194613. doi:10.1242/dev.194613

RESEARCH ARTICLE

Formal proof of the requirement of MESP1 and MESP2 in mesoderm specification and their transcriptional control via specific enhancers in mice

Rieko Ajima[1,2,3,*], Yuko Sakakibara[2], Noriko Sakurai-Yamatani[2], Masafumi Muraoka[1] and Yumiko Saga[1,2,3,*]

ABSTRACT

MESP1 and MESP2 are transcriptional factors involved in mesoderm specification, somite boundary formation and somite polarity regulation. However, Mesp quadruple mutant zebrafish displayed only abnormal somite polarity without mesoderm specification defects. In order to re-evaluate *Mesp1*/*Mesp2* mutants in mice, *Mesp1* and *Mesp2* single knockouts (KOs), and a *Mesp1*/*Mesp2* double KO were established using genome-editing techniques without introducing selection markers commonly used before. The *Mesp1*/*Mesp2* double KO embryos exhibited markedly severe mesoderm formation defects that were similar to the previously reported *Mesp1*/*Mesp2* double KO embryos, indicating species differences in the function of MESP family proteins. However, the *Mesp1* KO did not display any phenotype, including heart formation defects, which have been reported previously. We noted upregulation of *Mesp2* in the *Mesp1* KO embryos, suggesting that MESP2 rescues the loss of MESP1 in mesoderm specification. We also found that *Mesp1* and *Mesp2* expression in the early mesoderm is regulated by the cooperation of two independent enhancers containing T-box- and TCF/Lef-binding sites. Deletion of both enhancers caused the downregulation of both genes, resulting in heart formation defects. This study suggests dose-dependent roles of MESP1 and MESP2 in early mesoderm formation.

KEY WORDS: Mesoderm specification, MESP, Canonical Wnt signaling, CRISPR/Cas9

INTRODUCTION

The mesodermal cells are derived from the primitive streak (PS) during gastrulation in mouse development and continue to be produced in the tail bud from the anterior to posterior. These mesodermal cells give rise to the heart, head mesenchyme, blood, blood vessels, somites, kidney and limbs. In order to differentiate into different tissues, specific regulators for each tissue should be expressed in a spatiotemporal-specific manner in mesodermal cells. MESP1, a bHLH transcriptional factor, is the earliest marker for mesodermal cells. The *Mesp1* lineage, which is derived from the anterior mesoderm, gives rise to the heart and head mesenchyme, hematopoietic cells and blood vessels (Saga et al., 1996, 2000, 1999; Yoshida et al., 2008). *Mesp1*-null mutant mice exhibit heart morphology defects (Saga et al., 1999), suggesting that MESP1 is essential for cardiac formation. Although mice null for the *Mesp1* paralogue *Mesp2* did not exhibit anterior mesoderm formation defects (Saga et al., 1997), *Mesp1* and *Mesp2* double-null mice displayed the accumulation of undifferentiated mesoderm cells at the PS (Kitajima et al., 2000), suggesting that MESP1 and MESP2 have redundant functions in anterior mesoderm formation. Forced expression of MESP1 in mouse embryonic stem (ES) cells induced cardiac differentiation (Bondue et al., 2008; Chan et al., 2013; David et al., 2008; Lindsley et al., 2008), and introduction of the combination of MESP1 and other heart-specific transcriptional factors was proposed to reprogram cells into the cardiac lineage (Fu et al., 2013; Islas et al., 2012; Wada et al., 2013). This suggests that MESP1 and MESP2 are key regulators of anterior mesoderm differentiation. However, spatiotemporal regulation of *Mesp1* and *Mesp2* expression during early mesoderm formation has not been fully addressed. As *Mesp1* expression starts immediately after mesoderm cells are formed and is downregulated during gastrulation (Saga et al., 1996, 1999), it is possible that the regulation of *Mesp1* expression is coupled with PS formation and mesoderm progenitor cell specification. BMP from extra-embryonic tissue and epiblast Nodal have together been reported to induce the expression of *Wnt3* (Ben-Haim et al., 2006), then a WNT3 and NODAL positive-feedback loop determines where the PS is induced (Ben-Haim et al., 2006; Brennan et al., 2001; Rivera-Perez and Magnuson, 2005; Tortelote et al., 2013; Yoon et al., 2015). Wnt3 is soon downregulated at the PS (Liu et al., 1999). However, Wnt3a expression is induced at the PS (Takada et al., 1994), and canonical Wnt signaling is continuously activated at the PS and functions in the maintenance of mesodermal progenitors (Dunty et al., 2008; Garriock et al., 2015; Nowotschin et al., 2012; Takemoto et al., 2011). Activation of canonical Wnt signaling can induce mesodermal cells from ES cells (Chal et al., 2015; Gouti et al., 2014; Zhao et al., 2014). On the other hand, Nodal signaling activity is downregulated in the posterior part of the PS and the Nodal signal gradient in the PS has been proposed to specify a different lineage, as the anterior PS gives rise to the definitive endoderm and the posterior PS gives rise to the mesoderm (Arnold and Robertson, 2009; Morgani and Hadjantonakis, 2020; Robertson, 2014; Tam and Behringer, 1997; Tam and Loebel, 2007). Lefty2 is a downstream target of the Nodal pathway and functions as an inhibitor of Nodal (Meno et al., 1999; Saijoh et al., 2000; Sakuma et al., 2002). It also likely plays a role in the specification of mesodermal cells in the posterior PS. *Wnt3* conditional knockout (KO) in the epiblast, as well as *Lefty2*-null mice, exhibit defects in mesoderm migration from the PS and accumulation of mesodermal cells at the PS (Meno et al., 1999;

[1]Mammalian Development Laboratory, National Institute of Genetics, Research Organization of Information and Systems (ROIS), Yata 1111, Mishima, Shizuoka 411-8540, Japan. [2]Division for Development of Genetic-engineered Mouse Resource, Research Organization of Information and Systems (ROIS), Yata 1111, Mishima, Shizuoka 411-8540, Japan. [3]Department of Genetics, The Graduate University for Advanced Studies (SOKENDAI), Yata 1111, Mishima, Shizuoka 411-8540, Japan.

*Authors for correspondence (rajima@nig.ac.jp; ysaga@nig.ac.jp)

R.A., 0000-0001-9740-2660; Y. Saga, 0000-0001-9198-5164

Handling Editor: Patrick Tam
Received 30 June 2020; Accepted 20 September 2021

Development (2021) 148, dev194613. doi:10.1242/dev.194613

Table 1. F0 analysis of CRISPR/Cas9-mediated *Mesp1*/2 double knockout embryos

Dose of vectors	Number injected	Number reaching the two-cell stage	Number of embryos obtained		Gene modified (homo)		
			Phenotype	Number	*Mesp1*	*Mesp2*	Large deletion
5 ng/µl pX330/Mesp1-1 + 5 ng/µl pX330/Mesp2-2	485	238	Type I	65	44 (36)	16 (2)	0
			Type II	7	7 (6)	7 (7)	0
			Type III	6	6 (6)	6 (6)	1
5 ng/µl pX330/Mesp1-5 + 5 ng/µl pX330/Mesp2-5	496	311	Type I	34	23 (11)	18 (2)	0
			Type II	8	8 (5)	8 (6)	0
			Type III	6	6 (6)	6 (5)	0
Total	981	549	Type I	99	67 (47)	34 (4)	0
			Type II	15	15 (11)	15 (13)	0
			Type III	12	12 (12)	12 (11)	1

Homo indicates number of homozygously modified embryos. In these embryos, wild-type peaks were not observed by direct sequencing. The mutation did not necessarily cause a frame-shift. The large deletion column is the number of embryos with a 17.6 kb deletion between *Mesp1* and *Mesp2* genes.

Tortelote et al., 2013), which resembles the *Mesp1* and *Mesp2* double-null phenotype. It is therefore reasonable to hypothesize that tissue-specific expression of *Mesp1* and *Mesp2* is regulated by the continuous activation of canonical Wnt and downregulation of Nodal signaling in the posterior PS.

In zebrafish, Mesp overexpression causes cells to differentiate into the cardiac lineage (Deshwar et al., 2016), suggesting conserved Mesp family functions in early mesoderm formation. However, quadruple Mesp mutant zebrafish had only somite polarity defects, not early mesoderm formation defects (Yabe et al., 2016). Furthermore, the targeting strategy for *Mesp2* affected the severity of *Mesp2*-null phenotypes. In particular, the targeting strategy using the PGK-neo cassette affected the expression of the neighbor gene *Mesp1* (Takahashi et al., 2007). In this study, we re-established *Mesp1* and *Mesp2* single or *Mesp1/Mesp2* double-null mutant mice without inserting the PGK-neo cassette using CRISPR/Cas9-mediated genome editing, and evaluated the spatiotemporal regulation of *Mesp1* expression during anterior mesoderm formation.

RESULTS

Generation of CRISPR/Cas9-mediated *Mesp1* and *Mesp2* KO mice

The previously reported *Mesp1/Mesp2* double knockout (dKO) mice lines were generated by integrating the PGK-neo cassette following the KO strategy (Kitajima et al., 2000). In order to establish *Mesp1/Mesp2* dKO mice without using the PGK-*neo* cassette, we used the CRISPR/Cas9 genome-editing technique. We designed two sets of guide RNAs (sgRNAs), (1) Mesp1-1 and Mesp2-2, and (2) Mesp1-5 and Mesp2-5, to target both *Mesp1* and *Mesp2* genes simultaneously. We designed the sgRNAs upstream of the basic helix-loop-helix (bHLH) domain to create functionally null MESP1 and MESP2 proteins if a frame-shift occurred as the result of an indel caused by non-homologous end-joining (NHEJ) (Fig. S1A). Initially, we conducted F0 analyses. The bicistronic expression vectors expressing hCas9 mRNA and sgRNA for *Mesp1* and *Mesp2* (Table 1) were injected into fertilized eggs, and embryos were recovered at embryonic day (E) 9.5. The embryos were categorized into three groups by their phenotypes: type I exhibited normal morphology (Fig. 1A: n=99); type II displayed an ambiguous somite boundary, similar to *Mesp2* KO embryos (Fig. 1B: n=15); and type III embryos were completely disorganized, with traces of a head fold (HF)-like structure and allantois, and no posterior structure, similar to *Mesp1/Mesp2* dKO mutants (Fig. 1C: n=12). We observed no embryos with the double-heart phenotype expected for the *Mesp1*-single null mutant (Saga et al., 1999). The genotypes of embryos were confirmed by sequencing (Table S1). Type I contained *Mesp1*-null mutants caused by a frame-shift in both alleles. This suggests that *Mesp1*-null embryos developed normally, which is inconsistent with the previous report. Type I also contained homozygously modified *Mesp2* mutants. However, in most cases, the mutation contained only a small indel without a frame-shift. Type II contained *Mesp2* mutants with frame-shifts in both alleles, with at least one functional *Mesp1* allele. Type III embryos contained homozygous frame-shift mutations for both *Mesp1* and *Mesp2* (Table S1), confirming that the most severe phenotype was caused by the dKO mutation of *Mesp1* and *Mesp2*. The phenotype of Type II embryos was further analyzed by the expression of *Uncx4.1*, a caudal somite marker, and *T*, a presomitic mesoderm marker (Fig. S2). Most Type II embryos displayed a caudalized somite phenotype similar to previously reported *Mesp2* KO embryos with variable severity. This variable severity may have been caused by the mosaicism of F0 mutants (Table S1). Although we used two sets of sgRNAs for *Mesp1* and *Mesp2*, the mutation frequency in the *Mesp2* gene was low in both

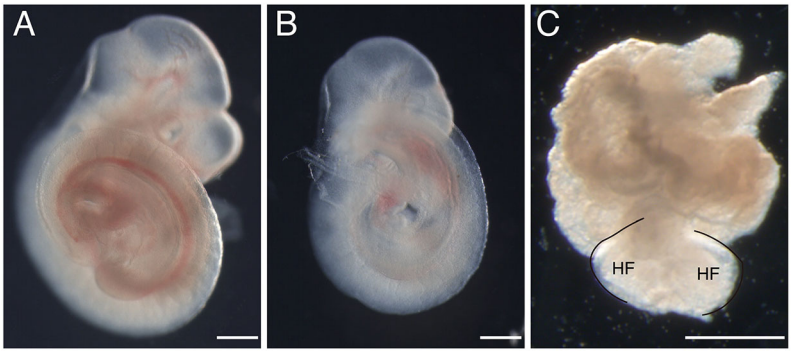

Fig. 1. Representative phenotypes of CRISPR/Cas9-mediated *Mesp1*/*Mesp2* double KO F0 embryos at E9.5. (A) Type I embryo displaying normal morphology. (B) Type II embryo displaying somite boundary formation defects similar to *Mesp2* KO. (C) Type III embryo displaying a head fold (HF)-like structure with a yolk sac. Scale bars: 500 µm.

Development (2021) 148, dev194613. doi:10.1242/dev.194613

Table 2. Establishment of CRISPR/Cas9-mediated *Mesp1*/*2* double knockout mice

Dose of vectors	Number injected	Number reaching the two-cell stage	Number of pups obtained	Gene modified (homo)	
				Mesp1	*Mesp2*
2 ng/µl pX330/Mesp1-1+2 ng/µl pX330/Mesp2-1	181	108	8	2 (0)	4 (0)
1 ng/µl pX330/Mesp1-5+1 ng/µl pX330/Mesp2-5	184	120	12	6 (0)	5 (0)

Homo indicates number of homozygously modified embryos. From the founders shown in the table, we established and maintained the following mutant lines: $Mesp1^{\Delta 2bp}$, $Mesp1^{\Delta 17bp}$, $Mesp2^{\Delta 53bp}$, $Mesp2^{+1bp}$, $Mesp2^{\Delta 1bp}$, $Mesp2^{\Delta 5bp}$, $Mesp2^{\Delta 21bp}$, $Mesp1^{\Delta 14bp}$;$Mesp2^{\Delta 27bp}$ and $Mesp1^{+1b}$;$Mesp2^{\Delta 10bp}$.

cases. In order to address the possibility that the *Mesp1* locus is more favorably mutated by the CRISPR/Cas9 technique than by the *Mesp2* locus, the bicistronic expression vectors expressing hCas9 mRNA and sgRNA for *Mesp1* or *Mesp2* were separately injected into fertilized eggs, and embryos were recovered at embryonic day (E) 9.5 (Table S2). Among the 20 embryos obtained by pX330/Mesp2-2 injection, all contained the indel mutation and 19 were homozygously mutated. This high frequency was similar to that seen in response to pX330/Mesp1-1 injection, in which we obtained 10 embryos, including eight with homozygous mutations. On the other hand, of 26 embryos obtained by pX330/Mesp2-5 injection, 19 were mutants, but only four had homozygous mutations (Table S2). The target sites of Mesp2-2 and Mesp2-5 sgRNAs are only 36 bp apart (Fig. S1A), suggesting that the efficiency of mutation by these sgRNAs is not regulated by epigenetic modification of the locus, but simply reflects the double-strand break efficiency. We injected pX330/Mesp1-1 and pX330/Mesp2-2 together again, and the efficiency at each locus was similar to that when injected separately (Table S2).

Establishment of *Mesp* mutant mice by genome editing

To analyze the phenotypes of the mutants in more detail, *Mesp1* and *Mesp2* KO lines were established using the CRISPR/Cas9 technique (Tables 2 and 3). $Mesp1^{\Delta 2bp/\Delta 2bp}$, $Mesp1^{\Delta 17bp/\Delta 17bp}$ and $Mesp1^{\Delta 573bp/\Delta 573bp}$ mice developed normally and were fertile, confirming that *Mesp1* is dispensable as long as the *Mesp2* allele remains intact. We obtained several types of *Mesp2* KO, including $Mesp2^{\Delta 53bp/\Delta 53bp}$, $Mesp2^{+1bp/+1bp}$, $Mesp2^{\Delta 1bp/\Delta 1bp}$ and $Mesp2^{\Delta 5bp/\Delta 5bp}$. The CRISPR/Cas9-mediated *Mesp2* KO embryos displayed phenotypes similar to those previously reported, such as upregulated *Mesp1* expression compared with controls at the newly forming somite boundary (Fig. 2A,D,G), caudalized somites (Fig. 2E,H, Fig. S3B,C), and fused pedicles and laminae of the neural arches (Fig. 2F,I). Embryos with a few nucleotide deletions without frame-shifts in *Mesp2* ($Mesp1^{\Delta 14bp/\Delta 14bp}$; $Mesp2^{\Delta 27bp/\Delta 27bp}$ and $Mesp2^{\Delta 21bp/\Delta 21bp}$) demonstrated normal development similar to controls (Fig. 2A-C,J-L, Fig. S3A,D), which was likely due to intact bHLH domains in these mutant embryos. We also established *Mesp1*/*Mesp2* dKO mouse lines ($Mesp1^{+1bp/+1bp}$;$Mesp2^{\Delta 10bp/\Delta 10bp}$ and $Mesp1^{\Delta 573bp/\Delta 573bp}$; $Mesp2^{\Delta 4bp/\Delta 4bp}$). Previously reported *Mesp1*/*Mesp2*-null phenotypes at the gastrulation stage (Kitajima et al., 2000), such as the accumulation of mesodermal cells around the PS (Fig. 3A-D) and loss of *Lefty2* expression (Fig. 3E,F), were also recapitulated in the dKO embryos. Furthermore, *Eomes*, *Fgf8* and *Wnt3*, which are expressed in the mesoderm at the gastrulation stage, were upregulated in the mesoderm of *Mesp1*/*Mesp2* dKO embryos (Fig. 3G-L). However, *Wnt3a*, which is expressed in the mesoderm later than *Wnt3*, was not expressed in the mesoderm of *Mesp1*/*Mesp2* dKO embryos (Fig. 3M,N). The expression of the epithelial-mesenchymal transition (EMT) marker *Snai1* was downregulated and restricted to the PS in *Mesp1*/*Mesp2* dKO embryos (Fig. 3O,P). This suggested that the mesodermal tissue in *Mesp1*/*Mesp2*-null embryos accumulated at an early mesodermal state and was prevented from further differentiation. Therefore, *Mesp1* and *Mesp2* are required for proper mesoderm formation in mouse but not in zebrafish.

Mesp1 KO mice display variable phenotypes depending on the targeting strategies

We found that *Mesp1*-null mice generated by genome editing had no abnormalities, suggesting that the phenotypes of *Mesp1* KO mice observed previously were caused by the PGK-neo cassette used for targeting. To address this possibility, we removed the PGK-neo cassette from the $Mesp1^{Neo}$ allele using CRISPR/Cas9-mediated genome editing with Mesp1-5′ and Mesp1-3′-2 sgRNAs (Fig. S1, Fig. 4A), and designated this as the $Mesp1^{\Delta Neo}$ allele. $Mesp1^{Neo/Neo}$ embryos displayed bifurcation of the cardiac primordia, as previously reported (Fig. 4B) (Saga et al., 1996). However, $Mesp1^{\Delta Neo/\Delta Neo}$ embryos had correctly looped single-tube hearts at a similar stage (Fig. 4C) to controls (Fig. 4A). Furthermore, $Mesp1^{\Delta Neo/\Delta Neo}$ mice developed normally and were fertile. We also made a new *Mesp1-Cre* line with a floxed PGK-neo cassette. This line was generated by almost the same strategy as the $Mesp1^{Cre}$ line previously produced (Saga et al., 1999), but the PGK-neo cassette was floxed and removed to produce $Mesp1^{Cre\Delta Neo}$ (Fig. S4A). The homozygous *Mesp1-Cre* mice exhibited severe heart developmental defects similar to or even more severe than those in the *Mesp1*-null embryo, in which *Mesp1* was replaced with the PGK-neo cassette (Lescroart et al., 2018; Saga et al., 1999). Similar to the $Mesp1^{\Delta Neo/\Delta Neo}$

Table 3. Establishment of CRISPR/Cas9-mediated $Mesp1^{Lefty2}$ knock-in mice

Dose of vectors	Number injected	Number reaching the two-cell stage	Number of pups obtained	Gene modified	
				Mesp1 (KI)	*Mesp2*
50 ng/µl Mesp1-1 gRNA, 50 ng/µl Mesp1 exon1-3′ gRNA, 1 ng/µl pX330/Mesp2-5, 10 ng/µl $Mesp1^{Lefty2}$ TV (circular) and 100 ng/µl Cas9 mRNA	102	87	17	15 (0)	7
50 ng/µl Mesp1-1 gRNA, 50 ng/µl Mesp1 exon1-3′ gRNA, 1 ng/µl pX330/Mesp2-5, 50 ng/µl $Mesp1^{Lefty2}$ TV (ssDNA), 100 ng/µl Cas9 mRNA and 100 ng/µl Cas9 protein	164	107	25	13 (1)	1

From the founders shown in the table, we established and maintained the following mutant lines: $Mesp1^{Lefty2}$, $Mesp1^{\Delta 573bp}$ and $Mesp1^{\Delta 573bp}$;$Mesp2^{\Delta 4bp.}$

Development (2021) 148, dev194613. doi:10.1242/dev.194613

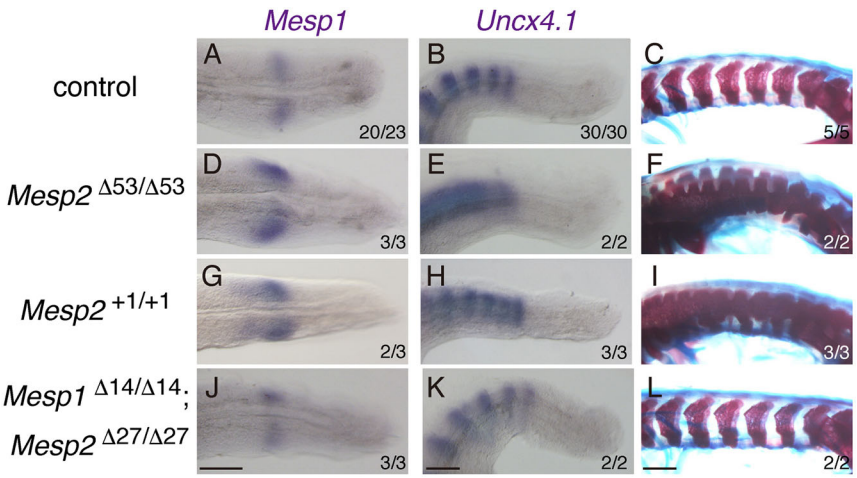

Fig. 2. CRISPR/Cas9-mediated *Mesp2* KO embryos reproduced previously reported *Mesp2* KO phenotypes. (A,B,D,E,G,H,J,K) Whole-mount *in situ* hybridization of embryos of the indicated genotype with the *Mesp1* probe (A,D,G,J) and *Uncx4.1* caudal somite marker probe (B,E,H,K) at E9.5. (C,F,I,L) Skeletal preparation of embryos of the indicated genotype at E18.5. *n* values indicate embryos showing the same expression pattern/number of embryos examined. Scale bars: in J, 200 µm for A,D,G,J; in K, 200 µm for B,E,H,K; in L, 1 mm for C,F,I,L.

case, $Mesp1^{CreΔNeo/CreΔNeo}$ mice also developed normally and were fertile. As MESP1 and MESP2 have redundant functions (Saga, 1998), *Mesp2* expression was examined in *Mesp1* KO embryos. In wild-type embryos, *Mesp2* expression was observed from the stage when gastrulation starts until the early-bud (EB) stage (Fig. 4D) and was downregulated around the late-bud (LB) stage (Fig. 4G). *Mesp2* expression became restricted to the lateral plate mesoderm around the early HF (EHF) stage (Fig. 4J) and was then further restricted at the boundary of newly forming somites (Fig. 4M). However, *Mesp2* expression was higher at the EB stage (Fig. 4F), and retained at the LB stage in $Mesp1^{ΔNeo/ΔNeo}$ (Fig. 4I) and $Mesp1^{CreΔNeo/CreΔNeo}$ embryos (Fig. S4C). This

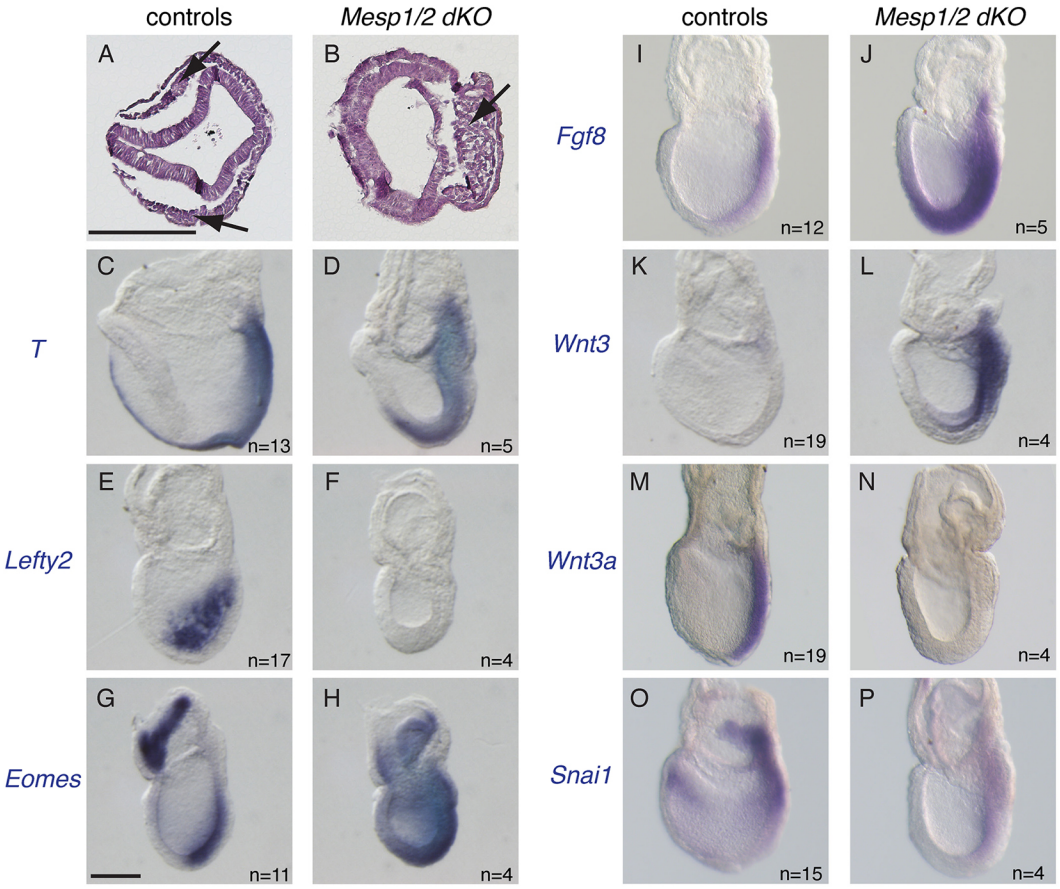

Fig. 3. CRISPR/Cas9-mediated *Mesp1*/*Mesp2* dKO embryos displayed mesoderm differentiation defects. (A,B) Hematoxylin and Eosin (H&E) staining of cross-sections of control (A) and *Mesp1*/*Mesp2* dKO (B) embryos at E7.5. Arrows indicate mesodermal cells that ingressed from the PS and migrated anteriorly in the control, but accumulated at the PS in the *Mesp1*/*Mesp2* dKO. (C-N) Whole-mount *in situ* hybridization of control (C,E,G,I,K,M,O) and *Mesp1*/*Mesp2* dKO ($Mesp1^{+1b/+1b}$; $Mesp2^{Δ10bp/Δ10bp}$ or $Mesp1^{Δ573bp/Δ573bp}$; $Mesp2^{Δ4bp/Δ4bp}$) (D,F,H,J,L,N,P) embryos at E7.5 with *T* (C,D), *Lefty2* (E,F), *Eomes* (G,H), *Fgf8* (I,J), *Wnt3* (K,L), *Wnt3a* (M,N) and *Snai1* (O,P) probes. Scale bars: 200 µm. *n* values indicate the number of embryos examined; all embryos of the same genotype displayed similar expression patterns to the representative embryos. *Wnt3* is expressed in the PS of earlier stage embryos than shown in K and is downregulated around the HF stage, as shown in K. Similarly sized *Mesp1*/*Mesp2* dKO embryos retained *Wnt3* expression (L).

Development (2021) 148, dev194613. doi:10.1242/dev.194613

upregulation was not observed in *Mesp1*$^{Neo/Neo}$ embryos (Fig. 4E,H), but *Mesp2* expression was retained at the LB stage, as previously reported (Kitajima et al., 2000), along with slight morphological defects, which may reflect a delay of mesodermal cell differentiation. All mutants exhibited the downregulation of *Mesp2* by the EHF stage (Fig. 4J-L, Fig. S4C), but its expression re-started again at the somitogenesis stage (Fig. 4M-O). In order to examine whether the upregulation of *Mesp2* expression in *Mesp1*$^{\Delta Neo/\Delta Neo}$ is sufficient to rescue *Mesp1*-null phenotypes, we conducted RNA-seq analysis using controls (*Mesp1*$^{\Delta Neo/+}$) and *Mesp1*$^{\Delta Neo/\Delta Neo}$ embryos at the EB and LB stages. Based on the pairwise scatterplot, regardless of the genotype and stage, the expression levels were highly correlated as the Pearson correlation coefficients were r>0.985 for all pairs (Fig. S5A). In the principal component analysis (PCA), the samples with the same stage or genotype were grouped together. However, the distance between biological replicates was similar to that between the same stage controls and *Mesp1*$^{\Delta Neo/\Delta Neo}$ samples. This suggested that the top 500 most variable genes were similar between the controls and *Mesp1*$^{\Delta Neo/\Delta Neo}$ (Fig. S5B). Indeed, only six genes, including *Mesp2*, at the EB stage and four genes and the LB stage were differentially expressed genes (DEGs) according to the comparison between control and *Mesp1*$^{\Delta Neo/\Delta Neo}$ samples (Fig. S5C, Table S3). The DEGs at the EB stage contained *Tdgf1* and *Eomes*, which are indispensable for PS formation (Ding et al., 1998; Russ et al., 2000; Xu et al., 1999). In order to determine whether the upregulation of these genes plays a role in rescuing *Mesp1*-null phenotypes, we examined their expression in control and *Mesp1*$^{\Delta Neo/\Delta Neo}$ embryos. However, their expression was unchanged between the control and *Mesp1*$^{\Delta Neo/\Delta Neo}$ embryos (Fig. S5D,E). *Mesp2* was the only gene among the DEGs whose expression was higher in both biological replicates of *Mesp1*$^{\Delta Neo/\Delta Neo}$ than in controls at both stages. It is

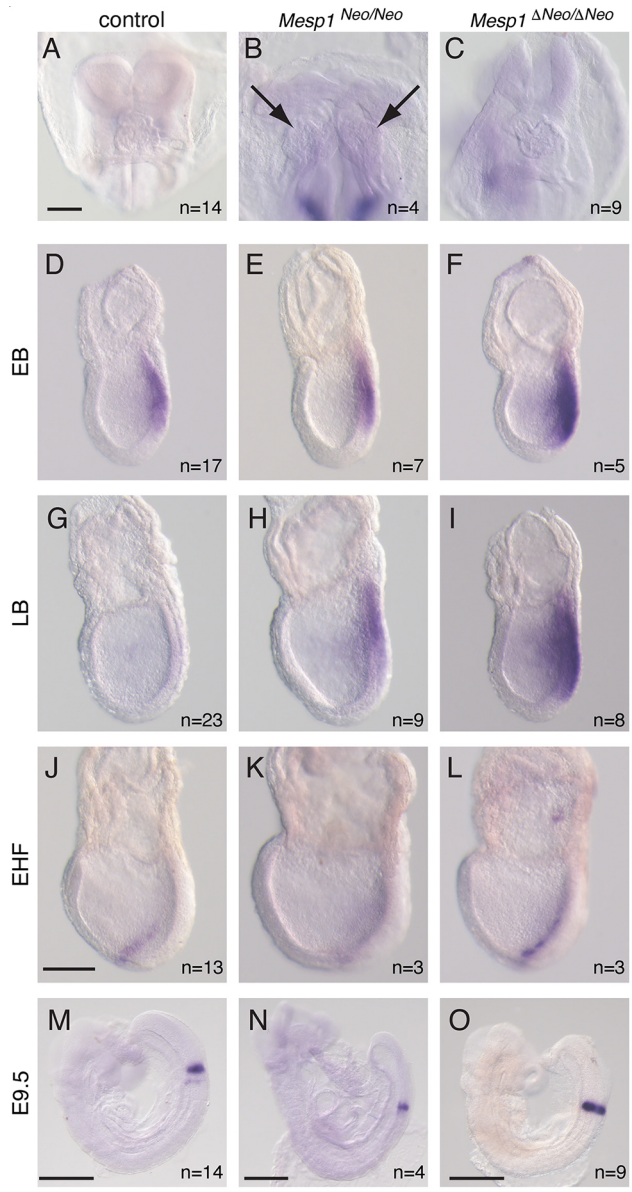

Fig. 4. *PGK-neo* cassette in the *Mesp1* locus prevents rescue expression of *Mesp2* in *Mesp1* KO embryos. (A-C) Frontal view of control (A), *Mesp1*$^{Neo/Neo}$ (B) and *Mesp1*$^{\Delta Neo/\Delta Neo}$ (C) embryos at the 7- to 8-somite stage. Arrows indicate bifurcation of the cardiac primordia. (D-O) Whole-mount *in situ* hybridization of control (D,G,J,M), *Mesp1*$^{Neo/Neo}$ (E,H,K,N) and *Mesp1*$^{Cre\Delta Neo/Cre\Delta Neo}$ (F,I,L,O) embryos at the EB stage (D-F), LB stage (G-I), EHF (J-L) and E9.5 (M-O) using the *Mesp2* probe. Staging was determined based on earlier work (Downs and Davies, 1993). Scale bars: 200 µm in A for A-C; 200 µm in J for J-L; 500 µm in M-O. *n* values indicate total embryos examined, except M-O (which indicate embryos examined at E8.5 and E9.5).

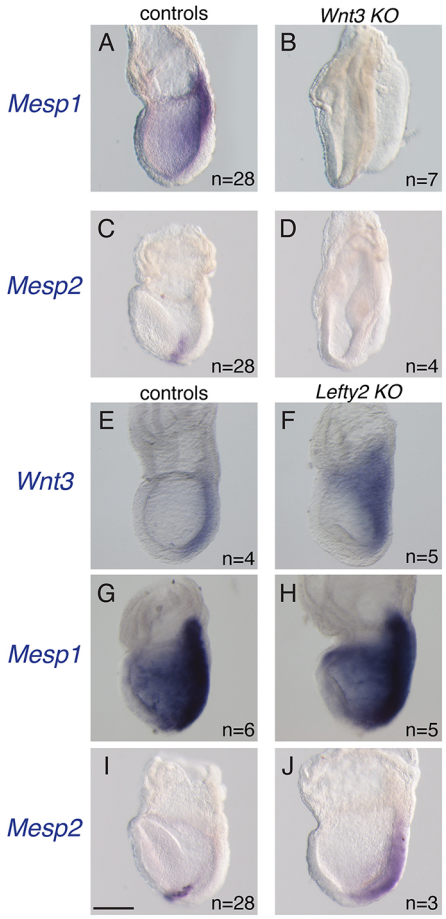

Fig. 5. *Lefty2* is downstream of MESP1/2. (A-D) Whole-mount *in situ* hybridization of control (A,C) and CRISPR/Cas9-mediated *Wnt3* KO embryos (B,D) with *Mesp1* (A,B) and *Mesp2* (C,D) probes. *Wnt3* KO had no PS, and lost *Mesp1* and *Mesp2* expression. (E-J) Whole-mount *in situ* hybridization of control (E,G,I) and CRISPR/Cas9-mediated *Lefty2* KO (F,H,J) embryos with *Wnt3* (E,F), *Mesp1* (G,H) and *Mesp2* (I,J) probes. Scale bar: 200 µm. *n* values indicate the number of embryos examined.

Development (2021) 148, dev194613. doi:10.1242/dev.194613

likely that the upregulation of *Mesp2* expression during early mesoderm formation rescued the phenotypes caused by deletion of *Mesp1*, but the PGK-*neo* cassette insertion prevented this rescue mechanism.

Forced *Lefty2* expression in the early mesoderm cannot rescue the early mesoderm formation defects in *Mesp1*/*Mesp2* dKO embryos

Although we confirmed that proper expression of *Mesp1* and *Mesp2* is essential for early mesoderm formation in mice, the regulation of *Mesp1* and *Mesp2* expression during the gastrulation stage is not well understood. As mesoderm specification requires continuous Wnt signaling activation and the suppression of Nodal signaling in the PS, *Mesp1* and *Mesp2* expression may be regulated by these signaling pathways. To assess this possibility, we established CRISPR/Cas9-mediated *Wnt3* KO and *Lefty2* KO mice, and examined *Mesp1* and *Mesp2* expression. The phenotype of the previously reported *Wnt3* null, which lacked the PS structure and expression of markers for the PS and early mesoderm (Liu et al., 1999), was recapitulated in the *Wnt3* KO generated by Cas9 (Fig. S6B,E,H). In the *Wnt3* KO, neither *Mesp1* nor *Mesp2* expression was observed (Fig. 5A-D). As reported previously, the *Lefty2* KO exhibited the accumulation of mesodermal cells around the PS (Meno et al., 1999). In the *Lefty2* KO embryos, *Wnt3* expression, as well as expression of the PS and early mesoderm markers, were upregulated in the thickened mesoderm (Fig. 5E,F and Fig. S6C,F,I), similar to in *Mesp1/Mesp2* dKO. However, *Mesp1* expression was unaffected (Fig. 5G,H) and *Mesp2* expression was retained in the *Lefty2* KO (Fig. 5I,J). Taken together with *Lefty2* expression being lost in *Mesp1/Mesp2* dKO (Fig. 3F), it is possible that *Lefty2* expression is regulated by MESP1 and MESP2 in the early mesoderm, and that it is essential for further mesoderm differentiation. To test this hypothesis, we established mice with *Lefty2* knocked into the *Mesp1* locus ($Mesp1^{Lefty2}$; Fig. S7). $Mesp1^{Lefty2/Lefty2}$ mice developed normally and were fertile. We then further established $Mesp1^{Lefty2/Lefty2}$;*Mesp2*-null mice. Although the $Mesp1^{Lefty2/Lefty2}$;*Mesp2*-null mice expressed *Lefty2* in the mesodermal cells at the gastrulation stage (Fig. 6A,B), the phenotypes were indistinguishable from those of *Mesp1/2* dKO mice (Fig. 6C-N). This suggested that *Lefty2* expression cannot rescue MESP1/2 loss in mesoderm differentiation.

Mesp1 expression in the early mesoderm is regulated by canonical Wnt signaling

We have previously reported that the enhancer to regulate *Mesp1* expression in the early mesoderm (EME) is located between 3.1 kb and 4.4 kb upstream of the *Mesp1* translational start site (Haraguchi et al., 2001). Further analysis of the EME using the VISTA tool revealed that there is an ∼340 bp highly conserved region (HCR1) among mammals, including mice, humans, dogs, cows and rats (Fig. S8A,B), which also contained the *Mesp1* presomitic mesoderm-specific enhancer (P1-PSME) with T- and E-boxes

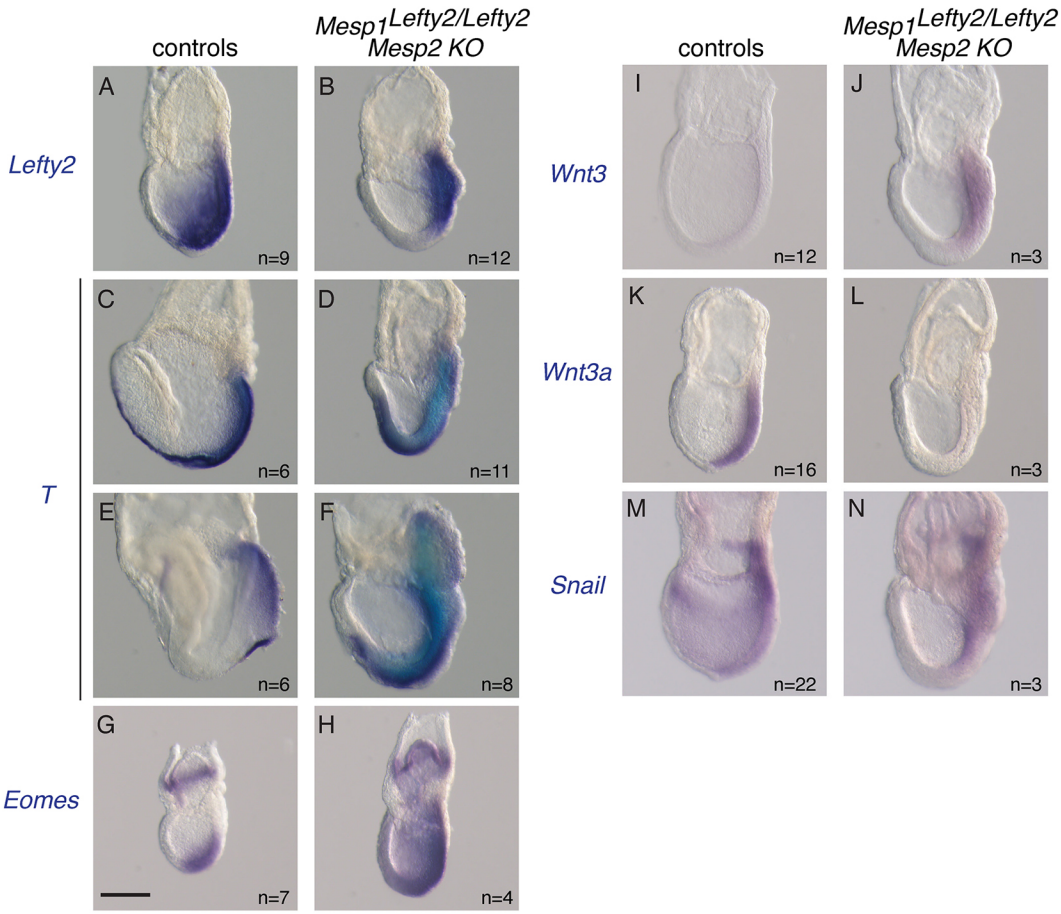

Fig. 6. The MESP1/2 downstream gene *Lefty2* cannot rescue the *Mesp1*/*Mesp2* dKO phenotypes. (A-N) Whole-mount *in situ* hybridization of control (A,C,E, G,I,K,M) and $Mesp1^{Lefty2/Lefty2}$; *Mesp2* KO (B,D,F,H,J,L,N) embryos with *Lefty2* (A,B), *T* (C-F), *Eomes* (G,H), *Wnt3* (I,J), *Wnt3a* (K,L) and *Snai1* (M,N) probes at E7.5 (A-D,G-N) and E8.5 (E,F). Scale bar: 200 µm. *n* values indicate the number of embryos examined.

Development (2021) 148, dev194613. doi:10.1242/dev.194613

(Fig. S8C) (Oginuma et al., 2008). As the Wnt and Nodal signaling pathways are essential for early mesoderm formation, *Mesp1* may be a target. We found a TCF/LEF-binding site (T/LBS2) in the HCR1, but no Smad-binding site (Fig. S8C). In the EME, there were three more TCF/LEF-binding sites, making a total of four TCF/LEF-binding sites (Fig. 7A). To evaluate the possibility that *Mesp1* is a direct target of the Wnt pathway, we examined enhancer activity using a transient transgenic assay. We introduced mutations into the four TCF/LEF-binding sites of the P1L-NB vector, which is a *lacZ* reporter containing the EME with the promoter region, designated as P1L-NB mutT/LBS. The P1L-NB reporter activity was not observed at streak stages (0 *lacZ*-positive embryos out of 15 transgenic embryos: 0/15), but was observed from bud stages in the mesodermal cells that emerged from the posterior PS (Fig. 7B: 8/14). The activity was maintained in the PSM from the headfold stages to early somitogenesis stages (Fig. 7C, 11/19). The reporter activity of P1L-NB mutT/LBS was markedly reduced compared with that of P1L-NB (Fig. 7D,E). As a previous report suggested that the sequence further upstream of the EME is also important for *Mesp1* expression (Oginuma et al., 2008), the HindIII-NcoI fragment was inserted to P1L-NB mutT/LBS, designated as P1L-HB mutT/LBS. However, its reporter activity was almost the same as that of P1L-NB mutT/LBS (Fig. 7F), indicating that the TCF/LEF sites are responsible for the enhancer activity. In order to further examine the role of canonical Wnt signaling in the enhancer activity, the enhancer and promoter fragments of P1L-NB and P1L-NB mutT/LBS were ligated into the Luciferase reporter plasmid, designated as P1Luc-NB and P1Luc-NB mutT/LBS, respectively. These reporters were transfected into ES cells, and their activities were examined with and without Wnt activation. P1Luc-NB reporter activity was upregulated upon canonical Wnt signaling activation by treatment with a GSK3 inhibitor, CHIR99021,

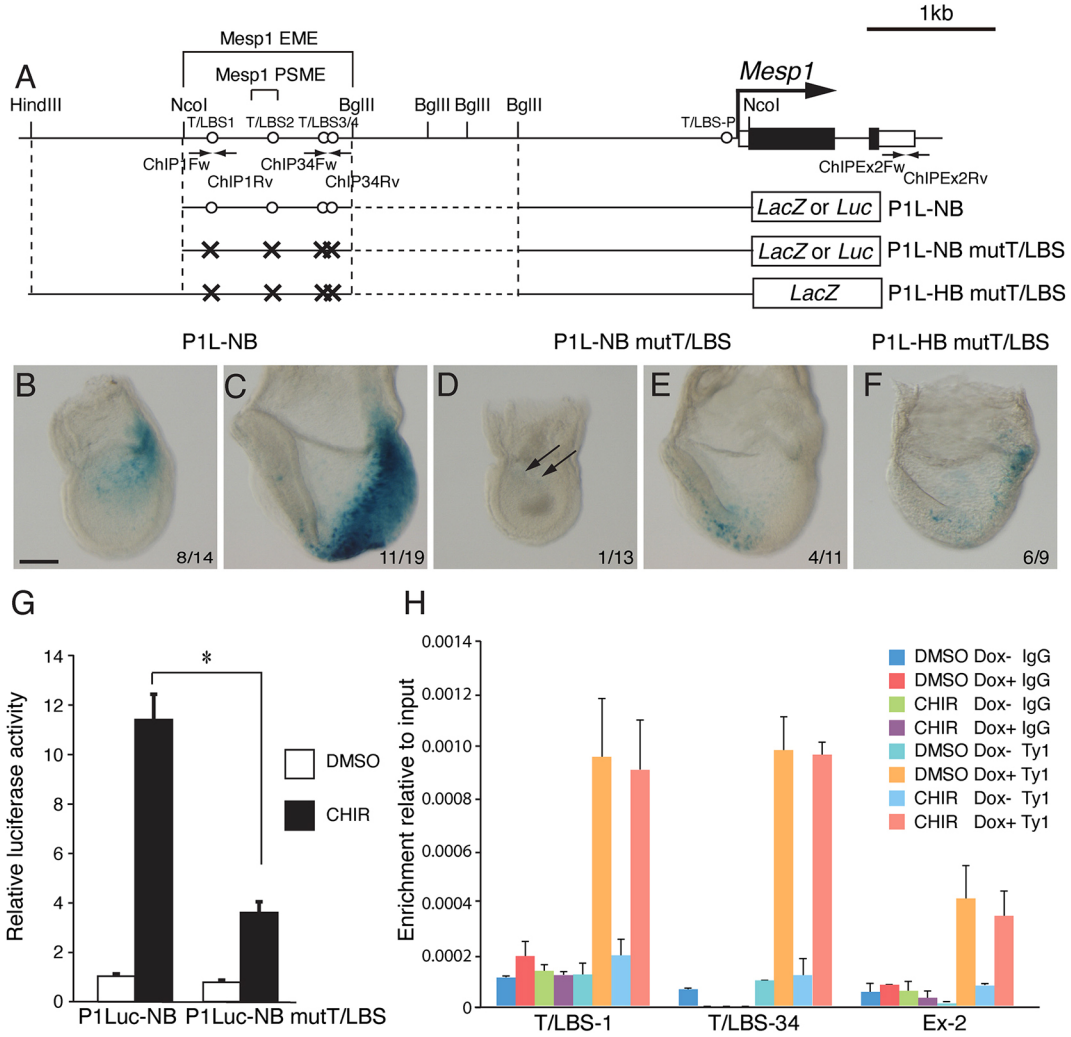

Fig. 7. *Mesp1* expression during early mesoderm formation was regulated by canonical Wnt signaling. (A) Schematic illustration of the *Mesp1* locus, *Mesp1* reporter constructs and primer positions for the ChIP assay. The positions of four TCF/Lef-binding sites (T/LBS) in the *Mesp1* early mesoderm enhancer (EME) and the previously reported TCF/LBS in the promoter (T/LBS-P) (Li et al., 2013) are indicated by circles. One of the T/LBSs is located in the *Mesp1* presomitic mesoderm enhancer (PSME). (B-F) X-gal staining of transient transgenic *Mesp1* reporter embryos. (B,C) Representative images of P1L-NB embryos. (D,E) Representative images of P1L-NB mT/LBS embryos. (F) Representative image of P1L-HB mT/LBS embryos. (B,D) Bud stage embryos. (C,E,F) Headfold stage or later stage embryos. Scale bar: 200 µm. Numbers indicate embryos that exhibited a similar expression pattern to that observed in transgene-positive embryos out of the total number of transgene-positive embryos. The remaining transgene-positive embryos exhibited no *lacZ* staining signal. Scale bar: 200 µm. (G) Luciferase assay of *Mesp1* reporters with or without T/LBS upon CHIR99021 treatment. Data are mean±s.d. $n=3$ (*$P<0.01$, unpaired, two-way Student's *t*-test). (H) ChIP assay using 3xTy1-Lef1 dox-inducible ES cell lines upon CHIR99021 treatment. Primer sets were designed at T/LBS-1, T/LBS-34 and the 3′UTR in exon 2 of *Mesp1* gene as a negative control. Data are mean±s.d. $n=3$.

Development (2021) 148, dev194613. doi:10.1242/dev.194613

whereas P1Luc-NB mutT/LBS reporter activity was one-third that of P1Luc-NB (Fig. 7G). We further conducted a ChIP assay to examine whether the direct binding of LEF1 to the putative binding sites is responsible for the activation. ES cells expressing LEF1 were examined with and without Wnt activation. As a result, LEF1 was able to interact with these TCF/LEF binding sites (Fig. 7H) regardless of Wnt activation. This suggested that *Mesp1* transcription is regulated through the TCF/LEF-binding sites in the EME upon canonical Wnt signaling activation.

Mesp1 EME is required for the maintenance of *Mesp1* expression during early mesoderm formation

In order to evaluate the EME activity for *Mesp1* expression during early mesoderm formation *in vivo*, we established EME-deleted mice (Figs S1B and S8A,B). *Mesp1* expression in the homozygously deleted embryos ($Mesp1^{EMEΔ1/Δ1}$) was not different from that in the controls at the EB stage (Fig. 8A,E). In the control embryos, *Mesp1* expression decreased around the EHF stage (Fig. 8C) and was restricted to newly forming somites in the somitogenesis stage (Fig. 8D). The *Mesp1* expression in $Mesp1^{EMEΔ1/Δ1}$ embryos decreased from the LB to EHF stage, earlier than in wild type (Fig. 8B,C,F,G), and almost no expression was observed at the somitogenesis stage (Fig. 8H), confirming that the EME also contained a somite-specific enhancer (PSME) for *Mesp1*. $Mesp1^{EMEΔ1/Δ1}$ mice were fertile and displayed no obvious phenotypes (Table S4). As *Mesp2* expression is upregulated in *Mesp1* null, we examined whether *Mesp1* downregulation in EME-deleted embryos causes the upregulation of *Mesp2* expression. However, *Mesp2* expression was unaltered compared with controls during early mesoderm formation (Fig. 8I-N), which suggested that the EME does not affect *Mesp2* expression, consistent with the previous report (Oginuma et al., 2008). Therefore, the maintenance, but not the onset, of *Mesp1* transcription, might be regulated through the EME. Further analysis is necessary to reveal which transcriptional factors regulate the onset of *Mesp1* expression in early mesoderm formation.

An enhancer, HCR2, regulates *Mesp2* expression during early mesoderm formation

As BAC-Tg experiments suggested that not only the EME, but also regions further upstream, including highly conserved region 2 (HCR2), is important for *Mesp1* expression in the early mesoderm (Oginuma et al., 2008), we further established mouse lines with deletion of upstream of the EME ($Mesp1^{EMEΔ2}$) and a larger deletion including a region upstream of the EME ($Mesp1^{EMEΔ1Δ2}$) (Fig. S1B). The *Mesp1* expression in $Mesp1^{EMEΔ2/Δ2}$ embryos did not differ from that in controls (Fig. 9A,B), and $Mesp1^{EMEΔ1Δ2/Δ1Δ2}$ embryos displayed similarly downregulated *Mesp1* expression to $Mesp1^{EMEΔ1/Δ1}$ embryos (Figs 8B,F and 9A,C). As this region is between *Mesp1* and *Mesp2* genes, we examined the possibility that *Mesp2* expression is regulated via this region. The *Mesp2* expression in $Mesp1^{EMEΔ2/Δ2}$ embryos did not differ from that in controls (Fig. 9D,E), but it was downregulated in $Mesp1^{EMEΔ1Δ2/Δ1Δ2}$ embryos (Fig. 9D,F). $Mesp1^{EMEΔ2/Δ2}$ mice were fertile and displayed no obvious phenotypes; however, $Mesp1^{EMEΔ1Δ2/Δ1Δ2}$ was embryonic lethal (Table S4). In order to examine the cause of lethality, we obtained embryos from $Mesp1^{EMEΔ1Δ2/+}$ intercrossing at E8.5 and E9.5 stages. $Mesp1^{EMEΔ1Δ2/Δ1Δ2}$ embryos at E8.5 (Fig. 9J,Q) exhibited developmental delay of ∼1 day with a less developed headfold and thickened mesodermal layer at the PS

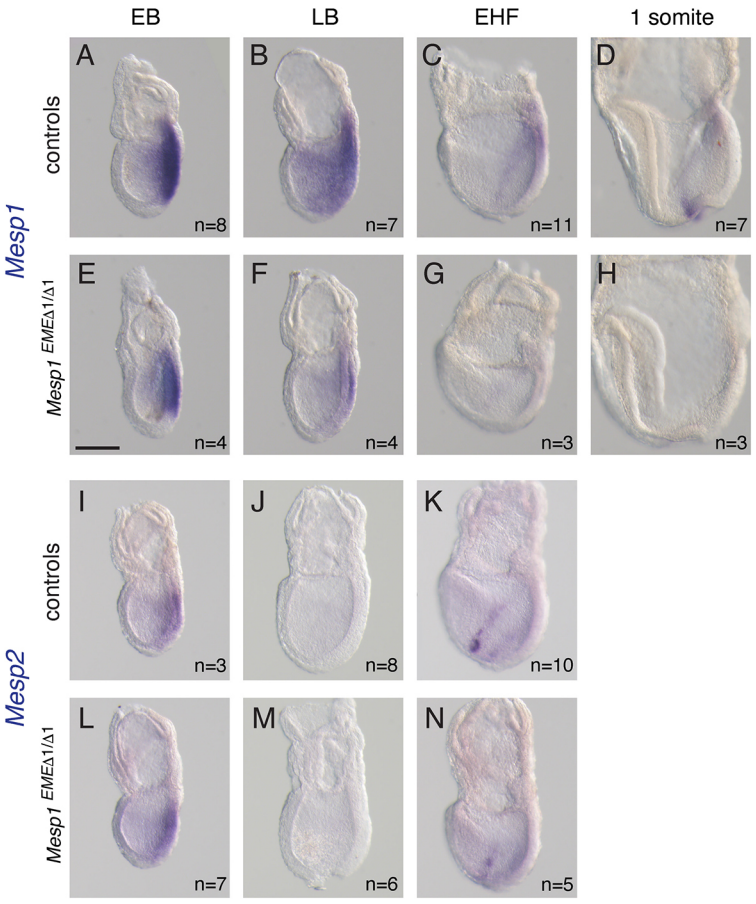

Fig. 8. Deletion of the *Mesp1* EME caused downregulation of *Mesp1* expression during early mesoderm formation. Whole-mount *in situ* hybridization of controls: wild-type (WT) and heterozygous (A-D,I-K), $Mesp1^{EMEΔ1/EMEΔ1}$ (E-H,L-N) embryos at indicated stages using *Mesp1* (A-H) and *Mesp2* (I-N) probes. Embryos exhibiting average intensities among the same genotype and same stage are shown. Staging was determined based on earlier work (Downs and Davies, 1993). Scale bar: 200 µm. Numbers indicate examined embryos. *n* values indicate the number of embryos examined

Development (2021) 148, dev194613. doi:10.1242/dev.194613

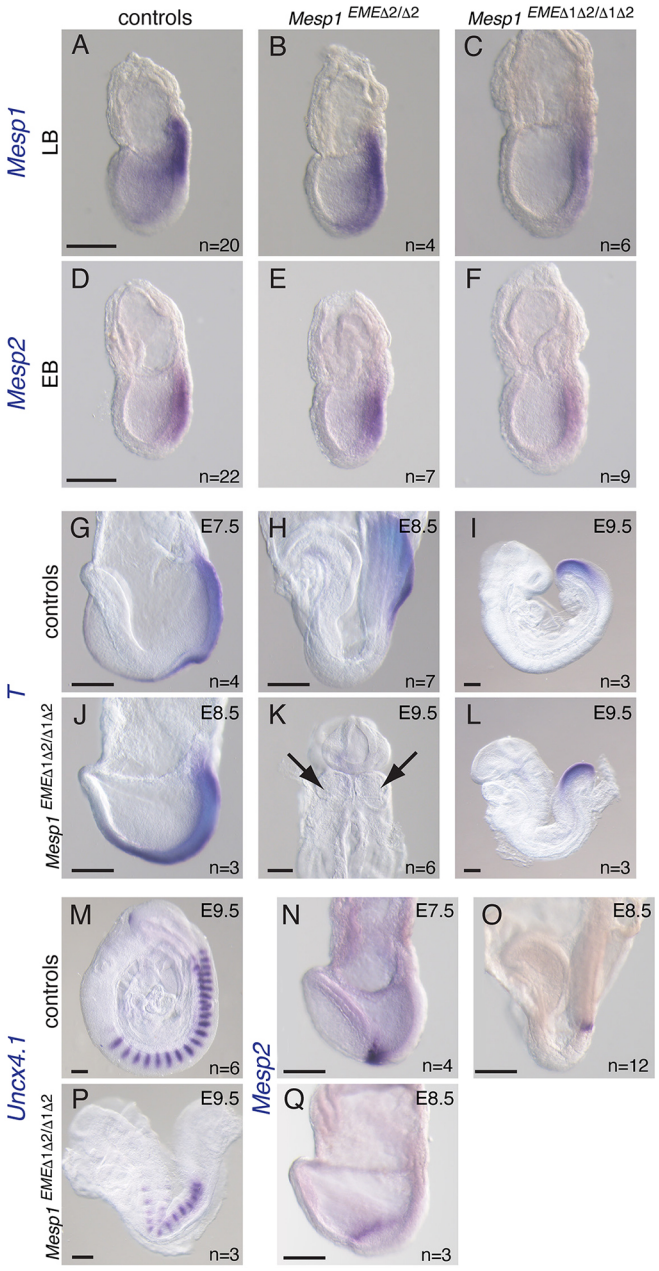

Fig. 9. Deletion of the HCR2 caused the downregulation of *Mesp2* expression during early mesoderm formation. (A-C) Whole-mount *in situ* hybridization of controls: wild type and heterozygous (A), *Mesp1*$^{EMEΔ2/EMEΔ2}$ (B), and *Mesp1*$^{EMEΔ1Δ2/EMEΔ1Δ2}$ (C) embryos at the LB stage using the *Mesp1* probe. (D-F) Whole-mount *in situ* hybridization of controls: wild type and heterozygous (D), *Mesp1*$^{EMEΔ2/EMEΔ2}$ (E), and *Mesp1*$^{EMEΔ1Δ2/EMEΔ1Δ2}$ (F) embryos at the EB stage using the *Mesp2* probe. (G-Q) Whole-mount *in situ* hybridization of controls (G-I,M-O) and *Mesp1*$^{EMEΔ1Δ2/EMEΔ1Δ2}$ (J-L,P,Q) embryos using the *T* probe (G-L), *Uncx4.1* probe (M,P) and *Mesp2* probe (N,O,Q). The embryos were dissected at E7.5 (G,N), E8.5 (H,J,O,Q) and E9.5 (I,K,L,M,P).

compared with similarly sized controls dissected at E7.5 (Fig. 9G,H). *Mesp1*$^{EMEΔ1Δ2/Δ1Δ\ 2}$ embryos at E9.5 had a smaller head and turning defect (Fig. 9L,P) compared with controls (Fig. 9I,M). In addition, *Mesp1*$^{EMEΔ1Δ2/Δ1Δ\ 2}$ embryos displayed bifurcation of the cardiac primordia (Fig. 9K), similar to *Mesp1*$^{Neo/Neo}$ embryos (Fig. 4B), which was likely the cause of lethality. Of note, the *Mesp1*$^{EMEΔ1Δ2/Δ1Δ\ 2}$ embryos at E9.5 had more than 10 somites, albeit smaller in size, which exhibited rostral-caudal polarity (Fig. 9M,P). Indeed, *Mesp2* was expressed in *Mesp1*$^{EMEΔ1Δ2/Δ1Δ\ 2}$ embryos at the lateral plate mesoderm, similar to controls (Fig. 9N,O,Q). This suggested that *Mesp2* expression is regulated through the combination of EME and HCR2 regions during early mesoderm formation, and the regulation is switched to another enhancer, likely a previously reported enhancer, during somitogenesis (Haraguchi et al., 2001; Yasuhiko et al., 2006, 2008) (Fig. S9).

DISCUSSION

MESP1 was previously proposed as a master regulator of cardiac progenitors. However, our CRISPR/Cas9-mediated *Mesp1* KO and *Mesp1-cre* mice without the PGK-neo cassette did not exhibit any phenotypes, including cardiac morphogenesis, although this does not mean that MESP1 is not important for cardiac formation. The CRISPR/Cas9-mediated *Mesp1/Mesp2* dKO confirmed the previous report (Figs 1 and 3) (Kitajima et al., 2000) that both MESP1 and MESP2 play important roles in early mesoderm formation. Although there is a report suggesting the presence of a few MESP1-specific target genes that can regulate the migration of cardiovascular progenitors (Chiapparo et al., 2016), MESP2 can fully rescue MESP1 functions directly or indirectly when *Mesp1* is knocked out. As MEPS1 and MESP2 are both important for early mesoderm formation, compensatory mechanisms exist and are activated when each gene is knocked out. Indeed, *Mesp1* and *Mesp2* single mutant mice demonstrated expression changes for the other gene (Saga et al., 1999; Takahashi et al., 2005, 2007). The existence of a heterologous promoter like the PGK promoter was previously suggested to affect expression of neighboring genes (Fiering et al., 1995; Olson et al., 1996; Seidl et al., 1999; West et al., 2016). In the *Mesp1/Mesp2* locus, insertion of the PGK-neo cassette into one gene may have affected the regulation of a neighboring gene, but it more likely prevented the rescue expression of the other, thereby making the phenotype more severe than that of the KO created without using the PGK-neo cassette. The mechanism of how *Mesp1/Mesp2* genes rescue each other when one is knocked out remains unknown. One possibility is that MESP1 and MESP2 act as transcription factors to suppress each other. To assess this possibility, we looked for putative E-boxes in the HCRs between *Mesp1* and *Mesp2* genes, where MESP1 and MESP2 may interact. We found one E-box in HCR1 (Fig. S8C) and two more in the EME. This is consistent with the report that MESP1 can interact around the EME in differentiated mouse ES cells (Bondue et al., 2008). However, deletion of the EME did not affect *Mesp2* expression (Fig. 8I-N, Fig. S1), suggesting that even if MESP1 interacts with the E-boxes in the EME and can suppress *Mesp2* transcription, its activity is not as strong as the rescue activity of the *Mesp2* gene in *Mesp1* KO mice. The other possibility is that there are common enhancers between *Mesp1* and *Mesp2* that compete for transcription factors. The T-box transcriptional factors EOMES and T/BRACHYURY have been reported to be the strongest candidate activators of *Mesp1* and *Mesp2* expression during early mesoderm formation. RNA-seq analyses revealed that *Mesp1* and *Mesp2* expression was repressed in the differentiating *Eomes* and *T* double KO ES cells (Tosic et al., 2019), and that EOMES and T/BRACHYURY directly interacted with the T-box in the *Mesp1* and *Mesp2* promoter and EME of *Mesp1* to regulate *Mesp1* and *Mesp2* expression (Costello et al., 2011; David et al., 2011; Tosic et al., 2019; van den Ameele et al., 2012). We looked for putative T-boxes in the HCRs between *Mesp1* and *Mesp2* genes. In addition to the previously reported T-boxes, we found two additional T-

Development (2021) 148, dev194613. doi:10.1242/dev.194613

boxes in HCR2 and HCR3 (Figs S8D,E and S9). Their positions were consistent with the ChIP-seq data using antibodies against EOMES and T/BRACHYURY in differentiating ES cells (Tosic et al., 2019). This suggested that *Mesp1* and *Mesp2* genes share EOMES and T/BRACHYURY for their activation at the early mesoderm formation stage through several shared T-boxes. A recent study revealed that once the promoter of a gene is removed or mutated, the enhancer for the gene can be used to activate the neighboring genes (Oh et al., 2021). Similar to this case, in the *Mesp1* and *Mesp2* loci, once one gene is knocked out, EOMES and T/BRACHYURY are no longer used for activation, and the other gene can use them via shared enhancers to promote its expression. This is consistent with results from our study. Deletion of the EME downregulated only *Mesp1* expression (Fig. 8A-H, Fig. S1), whereas simultaneous deletion of the EME and HCR2 also downregulated *Mesp2* expression during the early mesoderm formation stage (Fig. 9D-F, Fig. S1). This suggested that the EME is shared between *Mesp1* and *Mesp2* genes, and the T-box in the HCR2 is also important for *Mesp2* gene expression. Importantly, removing both enhancers resulted in similar cardiac morphological abnormality to that in $Mesp1^{Neo/Neo}$ embryos (Figs 4B and 9K). The total amount of MESP1 and MESP2 decreased in $Mesp1^{EMEΔ1Δ2/Δ1Δ2}$ and $Mesp1^{Neo/Neo}$ embryos, which caused the delay in mesodermal cell differentiation and migration out from the PS, affecting the development of head mesenchymal cells and the cardiac primordia. It is still unclear why the deletion of the EME affected *Mesp1* expression, but deletion of the EME or HCR2 region alone did not alter *Mesp2* expression (Figs 8A-N, 9D,E, Fig. S1). One possibility is that there are specific mechanisms for activating *Mesp2* expression through cooperative activation of these two enhancer regions. The other possibility is the distance between the promoter and enhancer, which has been proposed to affect transcriptional activity (Fukaya et al., 2016). As the EME and HCR2 are closer to the *Mesp1* promoter (Figs S1, S8 and S9), this may be sufficient to alter the expression level. However, the *Mesp2* promoter is further away from the EME and HCR2, and removal of the two enhancers, especially T-box binding sites, is needed to observe the alteration. Further studies, such as deletion of HCR3, may provide more insight into the mechanisms of compensation between *Mesp1* and *Mesp2* genes.

The mesodermal cells of *Mesp1/Mesp2* dKO were prevented from further differentiation and accumulated at the PS. Canonical Wnt and Nodal signaling is important to maintain the mesoderm progenitor cells, and must be downregulated for further differentiation of mesodermal cells. As the expression of T-box transcriptional factors *Eomes* and *T* in the PS is regulated by both Nodal and Wnt signaling pathways (Arnold et al., 2000; Barrow et al., 2007; Brennan et al., 2001; Simon et al., 2017; Yamaguchi et al., 1999), these signaling pathways may regulate *Mesp1* and *Mesp2* expression through the regulation of EOMES and BRACHYURY. *Lefty2* is a direct target of Nodal signaling and suppresses the signaling pathway, and *Lefty2* KO exhibited accumulation of the mesodermal tissue, similar to *Mesp1/Mesp2* dKO (Fig. 5C-F; Meno et al., 1999). *Lefty2* was also proposed as a downstream target of MESP1 and MESP2 (Fig. 3E,F; Costello et al., 2011; Kitajima et al., 2000; Lindsley et al., 2008). We therefore hypothesized that LEFTY2 is one of the factors responsible for early mesoderm specification. However, knock-in of *Lefty2* cDNA into the *Mesp1* locus did not rescue the *Mesp1/Mesp2* dKO phenotypes. Although *Lefty2* mRNA in $Mesp1^{Lefty2/Lefty2}$;*Mesp2* KO embryos was detected at comparable levels with those in controls (Fig. 6A,B), the LEFTY2 protein level may have been insufficient to be functional. On the other hand, it is more likely that MESP1 and MESP2 transcription factors induce other essential factor(s) for further differentiation, and this role cannot be substituted for by LEFTY2. LEFTY2 may regulate early mesoderm formation in parallel with MESP1 and MESP2. Detailed comparison between *Mesp1/Mesp2* dKO and *Lefty2* KO may reveal the mechanisms that specify early mesoderm differentiation.

In this study, we proposed that *Mesp1* can be regulated by the canonical Wnt signaling pathway via the EME. The transient transgenic assay using the *Mesp1* EME reporter revealed that mutations in TCF/LEF binding sites in the EME markedly reduced the reporter activity, but residual expression at the anterior part of the migrating mesoderm was observed (Fig. 7D). Deletion of the EME downregulated *Mesp1* expression only after the LB stage (Fig. 8A-H). This suggests that the canonical Wnt signaling pathway has a role not in the induction, but rather in the maintenance of *Mesp1* expression in the early mesoderm. As mentioned above, the EME also promotes *Mesp2* expression and it is possible that its expression is also regulated by the canonical Wnt signaling pathway via TCF/LEF-binding sites in the EME. MESP1 has been proposed to control the EMT by regulating the expression of *Snai1* (Lescroart et al., 2014; Lindsley et al., 2008), and we confirmed that *Snai1* was downregulated in *Mesp1/2* dKO embryos (Fig. 3O,P). Once the early mesoderm cells go through the EMT, the cells migrate out and away from the PS, which is the source of canonical WNTs. The downregulation of *Mesp1* after mesodermal cells migrate out of the PS may be caused by the reduced amount of WNT proteins received by cells.

As mentioned above, deletion of the two independent enhancers, EME and HCR2, caused the downregulation of *Mesp1* and *Mesp2* expression, and early mesoderm formation defects. However, this mutant formed segmented somites, suggesting that the transcriptional regulation of *Mesp1* and *Mesp2* is switched from the early mesoderm formation stage to the somitogenesis stage. Activity of the *Mesp2* enhancer in somitogenesis was identified around the transcriptional start site, and demonstrated to be regulated by a T-box transcriptional factor, TBX6, and the intracellular domain of Notch (NICD) (Haraguchi et al., 2001; Yasuhiko et al., 2006, 2008). The T-box in the EME was essential for *Mesp1* expression during somitogenesis (Oginuma et al., 2008), which is also activated by TBX6 (Sadahiro et al., 2018). Thus, the switch of transcriptional regulation of *Mesp1* and *Mesp2* from the early mesoderm formation stage to the somitogenesis stage can be due to the use of T-box binding sites by different T-box transcriptional factors. Further investigation is needed to understand how these two genes are activated and cooperatively function in early mesoderm formation, specification and somitogenesis.

MATERIALS AND METHODS

Mice

Mice carrying the $Mesp1^{Cre\ floxed\ Neo}$ allele were established as described previously (Saga et al., 1999) using the floxed pgk-neo cassette instead of the pgk-neo cassette. $Mesp1^{Cre\ floxed\ Neo}$ heterozygous mice were crossed with CAG-cre mice to remove the pgk-neo cassette. The resultant allele was designated as $Mesp1^{Cre\ ΔNeo}$. C57BL6, B6C3F1 and MCH strain mice were purchased from CLEA Japan. All mouse experiments were approved by the Animal Experimentation Committee at the National Institute of Genetics (Permit Number 27-13).

Preparation of sgRNA and hCas9

The bicistronic expression vector expressing sgRNA and hCas9 mRNA (pX330) (Cong et al., 2013) was purchased from Addgene (plasmid

Development (2021) 148, dev194613. doi:10.1242/dev.194613

#42230) pX330 was linearized with BbsI, gel purified, and then ligated with an annealed pair of oligos for Mesp1-1 (5′-caccGACTCGGAGCGCGGCTCGCAC-3′ and 5′-aaacGTGCGAGCCGCGCTCCGAGTC-3′), Mesp1-5 (5′-caccGCTACAGCGGACCCAATGGTC-3′ and 5′-aaacGACCATTGGGTCCGCTGTAGC-3′), Mesp1 exon1-3′ (5′-caccGCCGAGTCGCCGCAGAATCGT-3′ and 5′-aaacACGATTCTGCGGCGACTCGGC-3′), Mesp1EME5′ (5′-caccGCAGTTCGGTCTGGAGTAAGC-3′ and 5′-aaacGCTTACTCCAGACCGAACTGC-3′), Mesp1EME3′ (5′-caccGGAGGGGCTGCCTATCTTAC-3′ and 5′-aaacGTAAGATAGGCAGCCCCTCC-3′), Mesp1EMEΔ2 (5′-caccGTGGAGATCTCTGCCCGCGTC-3′ and 5′-aaacGACGCGGGCAGAGATCTCCAC-3′), Mesp2-2 (5′-caccGGCGCTGGGCGCGTTCGTCG-3′ and 5′-aaacCGACGAACGCGCCCAGCGCC-3′), Mesp2-5 (5′-caccGTAGTGCGCGTGCTACGGGC-3′ and 5′-aaacGCCCGTAGCACGCGCACTAC-3′), Lefty2 exon3-1 (5′-caccGCGTCCCCTGCGCCGCGAAA-3′ and 5′-aaacTTTCGCGGCGCAGGGGACGC-3′), Lefty2 exon3-3 (5′-caccGAGGGGACGCCGGACGGCAAG-3′ and 5′-aaacCTTGCCGTCCGGCGTCCCCTC-3′), Wnt3-182 (5′-caccGATGCACGAAGGCCGATTCAC-3′ and 5′-aaacGTGAATCGGCCTTCGTGCATC-3′), Wnt3-1229 (5′-GTCCTTGAGGAAGTCGCCAA-3′ and 5′-aaacTTGGCGACTTCCTCAAGGAC-3′) and Wnt3-1569 (5′-caccGCGTAGATGCGAATACACTCT-3′ and 5′-aaacAGAGTGTATTCGCATCTACGC-3′), and the resulting vectors were designated as pX330/Mesp1-1, pX330/Mesp1-5, pX330/Mesp1 exon1-3′, pX330/Mesp1EME5′, pX330/MespEME3′, pX330/Mesp1EMEΔ2, pX330/Mesp2-2, pX330/Mesp2-5, pX330/Lefty2 exon3-1, pX330/Lefty2 exon3-3, pX330/Wnt3-182, pX330/Wnt3-1229 and pX330/Wnt3-1569, respectively. pX330/Mesp1-1, pX330/Mesp1 exon1-3′, pX330/Mesp1EME5′-3, pX330/MespEME3′-1, pX330/Mesp1EMEΔ2-1 pX330/Lefty2 exon3-1, pX330/Lefty2 exon3-3, pX330/Wnt3-182, pX330/Wnt3-1229 and pX330/Wnt3-1569 were then used as a template to amplify the PCR product using the T7 promoter-attached forward primer for Mesp1-1 (5′-TTAATACGACTCACTATAGGGACTCGGAGCGCGGCTCGCAC-3′), Mesp1 exon1-3′ (5′-TTAATACGACTCACTATAGGGCCGAGTCGCCGCAGAATCGT-3′), Mesp1EME5′ (5′-TTAATACGACTCACTATAGGGGCAGTTCGGTCTGGAGTAAGC-3′), Mesp1EME3′ (5′-TTAATACGACTCACTATAGGGGGAGGGGCTGCCTATCTTAC-3′), Mesp1EMEΔ2 (5′-TTAATACGACTCACTATAGGGGTGGAGATCTCTGCCCGCGTC-3′), Lefty2 exon3-1 (5′-TTAATACGACTCACTATAGGGCGTCCCCTGCGCCGCGAAA-3′), Lefty2 exon3-3 (5′-TTAATACGACTCACTATAGGGAGGGGACGCCGGACGGCAAG-3′), Wnt3-182 (5′-TTAATACGACTCACTATAGGGATGCACGAAGGCCGATTCAC-3′), Wnt3-1229 (5′-TTAATACGACTCACTATAGGGTCCTTGAGGAAGTCGCCAA-3) and Wnt3-1569 (5′-TTAATACGACTCACTATAGGGCGTAGATGCGAATACACTCT-3′), respectively, and common reverse primer (5′-AAAAAAGCACCGACTCGGTG-3′). sgRNAs and hCas9 mRNA were synthesized as described previously (Ajima et al., 2017). The following Alt-R CRISPR-Cas9 crRNAs and tracrRNA were purchased from Integrated DNA Technologies: Mesp1-5′ crRNA (5′-AltR1-CUACAGCGGACCCAAUGGUCGUUUUAGAGCUAUGCU-AltR2-3′), Mesp1-3′-2 crRNA (5′-AltR1-CCAGGAUCUACUCCCUCCGAGUUUUAGAGCUAUGCU-AltR2-3′), Mesp2-2 crRNA (5′-AltR1- GGCGCUGGGCGCGUUCGUCGGUUUUAGAGCUAUGCU-AltR2-3′), Mesp2-5 crRNA (5′-AltR1-GUAGUGCGCGUGCUACGGGCGUUUUAGAGCUAUGCU-AltR2-3′) and Mesp2-6 crRNA (5′-AltR1-ACAAUAAGGAGGUGUCACCCGUUUUAGAGCUAUGCU-AltR2-3′). GeneArt Platinum Cas9 Nuclease was purchased from Thermo Fisher Scientific.

Construction of vectors

To establish the *Mesp1*^{Lefty2} targeting vector (TV), a 500 bp fragment upstream of the first ATG of the *Mesp1* gene as a 5′ long arm (LA), a 500 bp fragment downstream of the Mesp1 exon1-3′ gRNA recognition site as a 3′ long arm and a *Lefty2*-coding sequence fragment were amplified with KOD Fx Neo (TOYOBO) using C57BL6J genomic DNA as a template for the 5′ LA and 3′ LA, and pBS/Lefty2 plasmid as a template for the *Lefty2*-coding sequence. These three fragments with a XhoI-EcoRI-digested pBluescript SK+ fragment were joined using NEBuilder HiFi DNA assembly (New England Biolabs). Single-strand DNA of the *Mesp1*^{Lefty2} targeting vector was made using the Guide It long ssDNA Production System (TaKaRa) with phosphorylated T7 and T3 primers.

To establish the transgenes, mutations of the four putative TCF/Lef-binding sites (T/LBS) were introduced into the P1L-NB construct (Haraguchi et al., 2001) by PCR using the following primer sets with mutations, as underlined: mT/LBS-1 Fw (5′-GCATAGCACATTGGCGTAGCAAGGC-3′)+mT/LBS-1 Rv (5′-CGCCAATGTGCTATGCACAGTCCCT-3′); mT/LBS-2 Fw (5′-GGAGCGCCAATGGGCAGAGGAAGCAG-3′)+mT/LBS-2 Rv (5′-GCCCATTGGCGCTCCTTATCTGGCCAGT-3′); mT/LBS-3 Fw (5′-TGCCTAAATTGGCGGTTAATAAAATACAAC-3′)+mT/LBS-3 Rv (5′-CCGCCAATTTAGGCAGACATGTTT-3′); and mT/LBS-4 Fw (5′-AACCGCCAATTTCTATTAACAAGATGC-3′)+mT/LBS-4 Rv (5′-AATAGAAATTGGCGGTTGTATTTTATTAAC-3′). The construct with all four T/LBS mutations was designated as P1L-NB mutT/LBS. P1L-HB mutT/LBS was made by inserting the HindIII-NcoI fragment into the P1L-NB mutT/LBS construct. The HindIII-NotI fragment of P1L-NB, P1L-NB mutT/LBS or P1L-HB mutT/LBS was gel extracted using the QIAQuick Gel Extraction kit and used for embryo injection. To establish Luciferase reporters, NcoI fragments of P1L-NB and P1L-NB mutT/LBS were blunted and subcloned into the EcoRV site of the pGL4.10[luc2] vector (Promega).

To establish the 3xTy1-mLef expression plasmid, first 3xTy1 oligo DNAs (5′-CTAGCACCATGGAGGTGCACACCAACCAAGATCCGCTTGATGCTGAAGTTCATACAAACCAGGATCCCCTCGATGCCGAAGTCCATACTAATCAGGACCCACTGGACGCAA-3′ and 5′-AGCTTTGCGTCCAGTGGGTCCTGATTAGTATGGACTTCGGCATCGAGGGGATCCTGGTTTGTATGAACTTCAGCATCAAGCGGATCTTGGTTGGTGTGCACCTCCATGGTG-3′) were annealed and cloned into NheI and HindIII-digested pcDNA3.1 (Invitrogen). The resulting plasmid was designated as pcDNA3.1-3xTy1. The Lef1 cDNA fragment was amplified by PCR with HindIII-3xTy1-mLef1 Fw (5′-ACTGGACGCAAAGCTTCCCCAACTTTCCGGAGGAGG-3′) and 3xTy1-Lef1-NotI Rv (5′-TAGACTCGAGCGGCCGCTCAGATGTAGGCAGCTGTCATTCTGG-3′) primers with PrimeStar GXL DNA polymerase (TaKaRa) using cDNA of 3 µM CHIR99021-treated ES cells as a template. The fragment was subcloned into HindIII and NotI-digested pcDNA3.1-3xTy1 using In-fusion HD Mutagenesis (Clontech) and designated as pcDNA3.1-3xTy1-Lef1. The 3xTy1-Lef1 fragment was amplified by PCR with pcDNA3.1-3xTy1-Lef1 as a template, and subcloned into the XhoI-NotI-digested pPBhCMV_1HApA vector using In-fusion HD Mutagenesis (Clontech).

One-cell embryo injection

B6C3F1 (C57BL/6N×C3H/HeN) female mice were super-ovulated and mated with B6C3F1 males, and fertilized embryos were collected from oviducts. To establish *Mesp1*$^{\Delta Neo}$ lines, B6C3F1 (C57BL/6N×C3H/HeN) female mice were super-ovulated, and oocytes were collected and used for *in vitro* fertilization with sperm from a *Mesp1*$^{Neo/+}$ male.

To make gene-targeted mice, mixtures of different concentrations of pX330 vectors, sgRNA, hCas9 mRNA, GeneArt Platinum Cas9 Nuclease and a circular or single-strand targeting vector were dissolved in injection buffer [10 mM Tris-HCl and 0.1 mM EDTA (pH 7.5)], and injected into the pronucleus or cytoplasm of fertilized eggs in M2 medium (Sigma). For the transient transgenic assay, gel-purified transgene fragments were dissolved in injection buffer and injected into the pronucleus of fertilized eggs in M2 medium (Sigma). The injected zygotes were cultured in KSOM (Millipore) at 37°C under 5% CO_2 until the two-cell stage after 1.5 days. Thereafter, 20-32 two-cell stage embryos were transferred into the uterus of pseudo-pregnant MCH females at 0.5 dpc. Embryos were dissected on the indicated day or born naturally. Mouse lines established by CRISPR/Cas9-mediated genome editing were backcrossed several times with C57BL6 or B6C3F1 mice to eliminate any off-target mutations.

Genotyping

For direct sequencing of CRISPR/Cas9-mediated Mesp1/Mesp2 KO mice, ∼100 ng of the PCR products of the *Mesp1* allele with Mesp1 GT Fw (5′-AGTCCTGGCCATAGGTGCCTGACTTACT-3′)+Mesp1 GT Rv (5′-CGAGTGTGCGCATACGTAGCTTCTCC-3′) and *Mesp2* allele with

Development (2021) 148, dev194613. doi:10.1242/dev.194613

Mesp2-L5 (5′-GGGGACCACCTCACACCTTTAGTCCAG-3′)+Mesp2-R4 (5′-AGGCTAGGACCAAGCATCTGAGCCTGTG-3′) were treated with ExoSAP-IT (Affymetrix), reacted with the Big Dye Terminator v3.1 Cycle sequencing kit (Applied Biosystems) with *Mesp1* GT Fw and Mesp2-L4 (5′-CCGGTCCAGCTTCCCAGAGTCACACCAG-3′), respectively, according to the manufacturer's instructions, and then analyzed with the ABI 3130xl genetic analyzer (Applied Biosystems). The peaks were read manually or using TIDE web tool (https://tide.nki.nl). When the direct sequencing results of F0 analysis were unclear, the PCR products were subcloned into the pT7Blue-2 T-vector (Novagen) and sequenced with the T7 primer. For screening of the *Mesp1*^{Lefty2} targeted mice, the following PCR primer sets were used: Lefty2KI 5′Fw (5′-ACCAAAGCAGCA-GAGCTCCAGTC-3′)+Lefty2KI 5′Rv (-CTCAGGACCTGTTCCTCGGT-CATC-3′) and Lefty2KI 3′Fw (5′-GTGTTGCCTCAGAGATGACCTCC-TT-3′)+Lefty2KI 3′Rv (5′-AGGGTTGGAATGGTACAGTCTGGAT-3′). Genotyping primers for established mouse lines are listed in Table S5.

Whole-mount *in situ* hybridization

For embryonic day 9.5 (E9.5) and younger embryos, whole-mount *in situ* hybridization and probe synthesis were performed as previously described (Biris and Yamaguchi, 2014). For E10.5 embryos, the InsituPro system (M&S Instruments) was used for whole-mount *in situ* hybridization according to the manufacturer's instructions. For cloning of the Wnt3, Wnt3a and Eomes probes, total RNA from TT2 ES cells was isolated with the RNeasy mini kit (Qiagen), reverse transcription was conducted with SuperScript III (Invitrogen), cDNA was amplified with the primers listed below, and resulting PCR products were subcloned into SalI- and EcoRI-digested pBluescript SK+ using the In-Fusion HD cloning kit (Clontech). Primers used were: for the Wnt3 probe, Fw (5′-CCCCCTCGAGGTC-GACTTCTAATGGAGCCCCACCTGCTC-3′)+Rv (5′-CGGGCTGCAG-GAATTCTACTTGCAGGTGTGCACATCGTAGA-3′); for the Wnt3a probe, Fw (5′-CCCCCTCGAGGTCGACCGGCGATGGCTCCTCTCG-3′)+Rv (5′-CGGGCTGCAGGAATTCTCAGTGCGCGCGTTATGCC-3′); for the Eomes probe, Fw (5′-CCCCCTCGAGGTCGACTAAAGCATGCAG-TTGGGAGAGCAG-3′)+ Rv (5′-CGGGCTGCAGGAATTCTAGGGACT-TGTGTAAAAAGCATAATAAGC-3′). The other probes used in this study were prepared as described previously.

Skeletal preparation

E18.5 mouse embryos were fixed with 100% ethanol. For genotyping, PCR was performed using a piece of embryonic skin digested with proteinase K (Roche). Alcian Blue and Alizarin Red staining were performed as described previously (Saga et al., 1997; Takahashi et al., 2000).

RNA-seq analysis

E7.5 mouse embryos were dissected in ice-cold PBS and photographed, and a small piece of extra-embryonic tissue was trimmed for genotyping. The remaining tissue was frozen in liquid nitrogen and stored at −80°C until preparing total RNA. Two stage-matched embryos were lysed together with 500 µl of TRIzol Reagent (Thermo Fisher Scientific), heated at 55°C for 5 min, mixed with 100 µl of chloroform, centrifuged at 12,000 ***g*** at 4°C for 15 min and the supernatant collected. Next, 300 µl of ethanol was added to the supernatant, which was applied to an RNeasy MinElute Spin Column and total RNA was harvested according to the manufacturer's instructions (RNeasy Micro Kit, Qiagen). Total RNA was used to make the RNA-seq library using the KAPA Stranded mRNA-Seq Kit Illumina platform (KAPA) and barcoded with DNA adapters using the KAPA single-indexed adaptor kit (KAPA). Quality assessment was performed using the Agilent DNA1000 Kit (Agilent). The libraries were 100 bp pair-end and were sequenced on an Illumina Hiseq2500 (Illumina).

Bioinformatic analysis

For all libraries, low-quality sequences and adapters were trimmed or removed using Cutadapt (version 3.4) (Martin, 2011) with the following options: '-j 8 -m 36 -q 20 -a GATCGGAAGAGCACACGTCTGAACTCCAGTCAC'. The raw reads and processed reads were checked using FastQC (version 0.11.9, http://www.bioinformatics.babraham.ac.uk/projects/fastqc/). For preparation for mapping reads to the mouse reference genome, the ensembl mouse reference genome (release-102, Mus_musculus.GRCm38.dna.primary_assembly.fa.gz) and the gene annotation file in General Transfer Format (GTF) (Mus_musculus.GRCm38.102.gtf.gz) were downloaded from the ensembl ftp site (http://ftp.ensembl.org/), and non-chromosomal sequences (scaffolds) and the related annotation data were removed in the reference genome and the gene annotation GTF file, respectively. To increase the mapping accuracy of splicing reads, splice site and exon information were extracted from the gene annotation GTF file using the Python scripts hisat2_extract_splice_sites.py and hisat2_extract_exons.py, respectively, from the HISAT2 (version 2.2.1) package (Kim et al., 2015). The HISAT2 index files of the reference genome were built including the extracted genomic information using 'hisat2-build' command with options: '–ss' and '–exon'. Clean reads were then mapped to the HISAT2 index files using HISAT2 with default options. The obtained Sequence Alignment Map (SAM) files were sorted by genomic coordinates and converted to Binary Alignment Map (BAM) files using the SAMtools (version 1.13) (Li et al., 2009) 'sort' command with option: '-O BAM'. Raw read counts per gene were calculated using featureCounts (version 2.0.3) (Liao et al., 2014) with options: '-s 2 -T 8 -t exon -g gene_id -a Mus_musculus.GRCm38.102.gtf'. Only protein-coding genes were used for the downstream analysis of this study. Normalized counts and statistical values for differential gene expression analysis were calculated using the Bioconductor DESeq2 packages (version 1.32.0) (Love et al., 2014) in R (version 4.1.0) (https://cran.r-project.org/). To assess gene expression correlation between samples, the pair-wise scatterplot was produced using log2 (the normalized counts+1), the 'cor' function with the parameters "method='spearman' and use='pairwise.complete.obs'", and ggplot2 packages (version 3.3.5) (https://cran.r-project.org/web/packages/ggplot2/citation.html) in R. For PCA, the variance-stabilizing transformed (vst) normalized counts were calculated using the vst function of the DESeq2 with the default settings and PCA was performed with the top 500 most variable genes using the DESeq2 plotPCA function. To determine DEGs, MAplots for each comparison of sample groups (controls vs *Mesp1*$^{\Delta neo/\Delta neo}$ in EB or LB) were produced using the results of the DESeq2 analysis with ggplot2. DEGs were detected using the DESeq2 with the cut-off criteria of an adjusted *P*-value <0.01.

lacZ detection

X-gal staining of whole embryos to detect *lacZ* expression has been described previously (Saga et al., 1992). The embryos were subsequently examined for the presence of the transgene by PCR analysis with the following primer sets: P1LB-NB GT Fw (5′-GGTCCAGGTGGAGCAGACTGGACTA-3′)+LacZ-R5 (5′-GCCAGGGTTTTCCCAGTCACGACG-3′).

Luciferase assay

P1L-NB –luc or P1L-NB mutT/LBS-luc reporters with pRL-tk (Promega) internal control vector were transfected into feeder-depleted ES (TT2) cells with Lipofectamine 2000 (Invitrogen), and cultured with or without 3 µM CHIR99021 in DMEM supplemented with 10% FBS, 2 mM L-Glutamine, 1×MEM NEAA, 1×penicillin-streptomycin, 55 µM 2-mercaptoethanol, 3 mM adenosine, cytidine, guanosine, and uridine, and 1 mM thymidine. The samples were harvested 48 h after transfection and the Luciferase assay was conducted using the Dual Luciferase Reporter Assay System (Promega) according to the manufacturer's instructions.

Chromatin immunoprecipitation (ChIP) assay

To establish the DOX-inducible 3x*Ty1-Lef1*-expressing ES cell lines, ES (TT2) cells on Neo^{r} feeder cells were transfected with pPBhCMV-3xTy1-Lef1, pPBCAGrtTA-IN and pBase plasmids using Lipofectamine 2000 (Invitrogen), and then selected with 150 µg/ml of geneticin for 6 days and picked up. The feeder-depleted DOX-inducible ES cells were cultured on gelatin-coated plates with or without 3 µM CHIR99021 in DMEM supplemented with 10% FBS, 2 mM L-Glutamine, 1×MEM NEAA, 1×penicillin-streptomycin, 55 µM 2-mercaptoethanol, 3 mM adenosine, cytidine, guanosine and uridine, and 1 mM thymidine for 1 day, cultured with or without 1 µg/ml of doxycycline for 8 h. Chromatin was fixed with 1% formaldehyde for 10 min, and cells were then collected and washed with ice-cold PBS. The cell pellets were suspended with SDS lysis buffer [1%

SDS, 10 mM EDTA and 50 mM Tris (pH 8.1)], sonicated with Vibra-cell VCX-130 (80% amplitude, 15 s×20 times; Sonic) and centrifuged. The supernatants were aliquoted as the input, and the remaining supernatants were diluted ten times with dilution buffer [0.01% SDS, 1.1% TritonX-100, 1.2 mM EDTA, 16.6 mM Reis-HCl (pH 8.1) and 167 mM NaCl] with a Complete mini proteinase inhibitor tablet (Roche). The lysates were divided into two tubes and incubated with anti-Ty1 antibody (diagenode) or normal mouse IgG (Santa Cruz) overnight at 4°C with rotation, and with Dynabeads-ProteinG (Invitrogen)/sonicated salmon sperm DNA (BioDynamics laboratory) mixture for a further 4 h. The beads were washed with low-salt wash buffer [0.1% SDS, 1% Triton X-100, 2 mM EDTA, 20 mM Tris-HCl (pH 8.1) and 150 mM NaCl], high-salt wash buffer [0.1% SDS, 1% Triton X-100, 2 mM EDTA, 20 mM Tris-HCl (pH 8.1) and 500 mM NaCl], LiCl wash buffer [0.25 M LiCl, 1% IGEPAL-CA630, 1% deoxycholic acid, 1 mM EDTA and 10 mM Tris (pH 8.1)] and TE buffer [10 mM Tris-HCl and 1 mM EDTA (pH 8.0)] twice each. The precipitated complexes were eluted from the beads by incubation with elution buffer (1% SDS and 0.1 M $NaHCO_3$). To reverse histone-DNA crosslinks, a 1/25 volume of 5 M NaCl was added to the supernatants and inputs, and then incubated overnight at 65°C. These samples were treated with proteinase K and DNA was recovered by phenol/chloroform extraction followed by ethanol precipitation, and then used for real-time PCR (Thermal Cycler Dice, TaKaRa).

Acknowledgements
We are particularly thankful to Dr Kurumi Fukuda and Makoto Kiso (National Institute of Genetics, Japan) for technical support. We are grateful to Dr Hitoshi Niwa for providing pPBhCMV_1cHApA, pPBCAGrtTA-IN and pBase plasmids. We are grateful to Dr Atushi Toyoda (Advanced Genomics Center, National Institute of Genetics, Japan) for supporting RNA-seq analysis. We are grateful to Danelle Wright for editing the manuscript.

Competing interests
The authors declare no competing or financial interests.

Author contributions
Conceptualization: R.A., Y. Saga; Investigation: R.A., Y. Sakakibara, N.S.-Y.; Data curation: M.M.; Writing - original draft: R.A.; Writing - review & editing: Y. Saga; Supervision: Y. Saga; Funding acquisition: Y. Saga.

Funding
This work was supported by funding from the Transdisciplinary Research Integration Center of the Research Organization of Information and Systems of the Japan Society for the Promotion of Science.

Data availability
RNA sequencing raw data are available in the DDBJ database (http://trace.ddbj.nig.ac.jp/DRASearch) under accession number DRA012726, and processed data are available under accession number E-GEAD-452.

Peer review history
The peer review history is available online at https://journals.biologists.com/dev/article-lookup/doi/10.1242/dev.194613.

References
Ajima, R., Suzuki, E. and Saga, Y. (2017). Pofut1 point-mutations that disrupt O-fucosyltransferase activity destabilize the protein and abolish Notch1 signaling during mouse somitogenesis. *PLoS One* **12**, e0187248. doi:10.1371/journal.pone.0187248

Arnold, S. J. and Robertson, E. J. (2009). Making a commitment: cell lineage allocation and axis patterning in the early mouse embryo. *Nat. Rev. Mol. Cell Biol.* **10**, 91-103. doi:10.1038/nrm2618

Arnold, S. J., Stappert, J., Bauer, A., Kispert, A., Herrmann, B. G. and Kemler, R. (2000). Brachyury is a target gene of the Wnt/beta-catenin signaling pathway. *Mech. Dev.* **91**, 249-258. doi:10.1016/S0925-4773(99)00309-3

Barrow, J. R., Howell, W. D., Rule, M., Hayashi, S., Thomas, K. R., Capecchi, M. R. and McMahon, A. P. (2007). Wnt3 signaling in the epiblast is required for proper orientation of the anteroposterior axis. *Dev. Biol.* **312**, 312-320. doi:10.1016/j.ydbio.2007.09.030

Ben-Haim, N., Lu, C., Guzman-Ayala, M., Pescatore, L., Mesnard, D., Bischofberger, M., Naef, F., Robertson, E. J. and Constam, D. B. (2006). The nodal precursor acting via activin receptors induces mesoderm by maintaining a source of its convertases and BMP4. *Dev. Cell* **11**, 313-323. doi:10.1016/j.devcel.2006.07.005

Biris, K. K. and Yamaguchi, T. P. (2014). Two-color in situ hybridization of whole-mount mouse embryos. *Methods Mol. Biol.* **1092**, 17-30. doi:10.1007/978-1-60327-292-6_2

Bondue, A., Lapouge, G., Paulissen, C., Semeraro, C., Iacovino, M., Kyba, M. and Blanpain, C. (2008). Mesp1 acts as a master regulator of multipotent cardiovascular progenitor specification. *Cell Stem Cell* **3**, 69-84. doi:10.1016/j.stem.2008.06.009

Brennan, J., Lu, C. C., Norris, D. P., Rodriguez, T. A., Beddington, R. S. P. and Robertson, E. J. (2001). Nodal signalling in the epiblast patterns the early mouse embryo. *Nature* **411**, 965-969. doi:10.1038/35082103

Chal, J., Oginuma, M., Al Tanoury, Z., Gobert, B., Sumara, O., Hick, A., Bousson, F., Zidouni, Y., Mursch, C., Moncuquet, P. et al. (2015). Differentiation of pluripotent stem cells to muscle fiber to model Duchenne muscular dystrophy. *Nat. Biotechnol.* **33**, 962-969. doi:10.1038/nbt.3297

Chan, S. S.-K., Shi, X., Toyama, A., Arpke, R. W., Dandapat, A., Iacovino, M., Kang, J., Le, G., Hagen, H. R., Garry, D. J. et al. (2013). Mesp1 patterns mesoderm into cardiac, hematopoietic, or skeletal myogenic progenitors in a context-dependent manner. *Cell Stem Cell* **12**, 587-601. doi:10.1016/j.stem.2013.03.004

Chiapparo, G., Lin, X., Lescroart, F., Chabab, S., Paulissen, C., Pitisci, L., Bondue, A. and Blanpain, C. (2016). Mesp1 controls the speed, polarity, and directionality of cardiovascular progenitor migration. *J. Cell Biol.* **213**, 463-477. doi:10.1083/jcb.201505082

Cong, L., Ran, F. A., Cox, D., Lin, S., Barretto, R., Habib, N., Hsu, P. D., Wu, X., Jiang, W., Marraffini, L. A. et al. (2013). Multiplex genome engineering using CRISPR/Cas systems. *Science* **339**, 819-823. doi:10.1126/science.1231143

Costello, I., Pimeisl, I.-M., Drager, S., Bikoff, E. K., Robertson, E. J. and Arnold, S. J. (2011). The T-box transcription factor Eomesodermin acts upstream of Mesp1 to specify cardiac mesoderm during mouse gastrulation. *Nat. Cell Biol.* **13**, 1084-1091. doi:10.1038/ncb2304

David, R., Brenner, C., Stieber, J., Schwarz, F., Brunner, S., Vollmer, M., Mentele, E., Müller-Höcker, J., Kitajima, S., Lickert, H. et al. (2008). MesP1 drives vertebrate cardiovascular differentiation through Dkk-1-mediated blockade of Wnt-signalling. *Nat. Cell Biol.* **10**, 338-345. doi:10.1038/ncb1696

David, R., Jarsch, V. B., Schwarz, F., Nathan, P., Gegg, M., Lickert, H. and Franz, W.-M. (2011). Induction of MesP1 by Brachyury(T) generates the common multipotent cardiovascular stem cell. *Cardiovasc. Res.* **92**, 115-122. doi:10.1093/cvr/cvr158

Deshwar, A. R., Onderisin, J. C., Aleksandrova, A., Yuan, X., Burrows, J. T. A. and Scott, I. C. (2016). Mespaa can potently induce cardiac fates in zebrafish. *Dev. Biol.* **418**, 17-27. doi:10.1016/j.ydbio.2016.08.022

Ding, J., Yang, L., Yan, Y.-T., Chen, A., Desai, N., Wynshaw-Boris, A. and Shen, M. M. (1998). Cripto is required for correct orientation of the anterior-posterior axis in the mouse embryo. *Nature* **395**, 702-707. doi:10.1038/27215

Downs, K. M. and Davies, T. (1993). Staging of gastrulating mouse embryos by morphological landmarks in the dissecting microscope. *Development* **118**, 1255-1266.

Dunty, W. C., Jr, Biris, K. K., Chalamalasetty, R. B., Taketo, M. M., Lewandoski, M. and Yamaguchi, T. P. (2008). Wnt3a/beta-catenin signaling controls posterior body development by coordinating mesoderm formation and segmentation. *Development* **135**, 85-94. doi:10.1242/dev.009266

Fiering, S., Epner, E., Robinson, K., Zhuang, Y., Telling, A., Hu, M., Martin, D. I., Enver, T., Ley, T. J. and Groudine, M. (1995). Targeted deletion of 5'HS2 of the murine beta-globin LCR reveals that it is not essential for proper regulation of the beta-globin locus. *Genes Dev.* **9**, 2203-2213. doi:10.1101/gad.9.18.2203

Fu, J.-D., Stone, N. R., Liu, L., Spencer, C. I., Qian, L., Hayashi, Y., Delgado-Olguin, P., Ding, S., Bruneau, B. G. and Srivastava, D. (2013). Direct reprogramming of human fibroblasts toward a cardiomyocyte-like state. *Stem Cell Rep.* **1**, 235-247. doi:10.1016/j.stemcr.2013.07.005

Fukaya, T., Lim, B. and Levine, M. (2016). Enhancer control of transcriptional bursting. *Cell* **166**, 358-368. doi:10.1016/j.cell.2016.05.025

Garriock, R. J., Chalamalasetty, R. B., Kennedy, M. W., Canizales, L. C., Lewandoski, M. and Yamaguchi, T. P. (2015). Lineage tracing of neuromesodermal progenitors reveals novel Wnt-dependent roles in trunk progenitor cell maintenance and differentiation. *Development* **142**, 1628-1638. doi:10.1242/dev.111922

Gouti, M., Tsakiridis, A., Wymeersch, F. J., Huang, Y., Kleinjung, J., Wilson, V. and Briscoe, J. (2014). In vitro generation of neuromesodermal progenitors reveals distinct roles for wnt signalling in the specification of spinal cord and paraxial mesoderm identity. *PLoS Biol.* **12**, e1001937. doi:10.1371/journal.pbio.1001937

Haraguchi, S., Kitajima, S., Takagi, A., Takeda, H., Inoue, T. and Saga, Y. (2001). Transcriptional regulation of Mesp1 and Mesp2 genes: differential usage of

enhancers during development. *Mech. Dev.* **108**, 59-69. doi:10.1016/S0925-4773(01)00478-6

Islas, J. F., Liu, Y., Weng, K.-C., Robertson, M. J., Zhang, S., Prejusa, A., Harger, J., Tikhomirova, D., Chopra, M., Iyer, D. et al. (2012). Transcription factors ETS2 and MESP1 transdifferentiate human dermal fibroblasts into cardiac progenitors. *Proc. Natl. Acad. Sci. USA* **109**, 13016-13021. doi:10.1073/pnas.1120299109

Kim, D., Langmead, B. and Salzberg, S. L. (2015). HISAT: a fast spliced aligner with low memory requirements. *Nat. Methods* **12**, 357-360. doi:10.1038/nmeth.3317

Kitajima, S., Takagi, A., Inoue, T. and Saga, Y. (2000). MesP1 and MesP2 are essential for the development of cardiac mesoderm. *Development* **127**, 3215-3226. doi:10.1242/dev.127.15.3215

Lescroart, F., Chabab, S., Lin, X., Rulands, S., Paulissen, C., Rodolosse, A., Auer, H., Achouri, Y., Dubois, C., Bondue, A. et al. (2014). Early lineage restriction in temporally distinct populations of Mesp1 progenitors during mammalian heart development. *Nat. Cell Biol.* **16**, 829-840. doi:10.1038/ncb3024

Lescroart, F., Wang, X., Lin, X., Swedlund, B., Gargouri, S., Sànchez-Dànes, A., Moignard, V., Dubois, C., Paulissen, C., Kinston, S. et al. (2018). Defining the earliest step of cardiovascular lineage segregation by single-cell RNA-seq. *Science* **359**, 1177-1181. doi:10.1126/science.aao4174

Li, H., Handsaker, B., Wysoker, A., Fennell, T., Ruan, J., Homer, N., Marth, G., Abecasis, G., Durbin, R. et al. (2009). The sequence alignment/Map format and SAMtools. *Bioinformatics* **25**, 2078-2079. doi:10.1093/bioinformatics/btp352

Li, Y., Yu, W., Cooney, A. J., Schwartz, R. J. and Liu, Y. (2013). Brief report: Oct4 and canonical Wnt signaling regulate the cardiac lineage factor Mesp1 through a Tcf/Lef-Oct4 composite element. *Stem Cells* **31**, 1213-1217. doi:10.1002/stem.1362

Liao, Y., Smyth, G. K. and Shi, W. (2014). featureCounts: an efficient general purpose program for assigning sequence reads to genomic features. *Bioinformatics* **30**, 923-930. doi:10.1093/bioinformatics/btt656

Lindsley, R. C., Gill, J. G., Murphy, T. L., Langer, E. M., Cai, M., Mashayekhi, M., Wang, W., Niwa, N., Nerbonne, J. M., Kyba, M. et al. (2008). Mesp1 coordinately regulates cardiovascular fate restriction and epithelial-mesenchymal transition in differentiating ESCs. *Cell Stem Cell* **3**, 55-68. doi:10.1016/j.stem.2008.04.004

Liu, P., Wakamiya, M., Shea, M. J., Albrecht, U., Behringer, R. R. and Bradley, A. (1999). Requirement for Wnt3 in vertebrate axis formation. *Nat. Genet.* **22**, 361-365. doi:10.1038/11932

Love, M. I., Huber, W. and Anders, S. (2014). Moderated estimation of fold change and dispersion for RNA-seq data with DESeq2. *Genome Biol.* **15**, 550. doi:10.1186/s13059-014-0550-8

Martin, M. (2011). Cutadapt removes adapter sequences from high-throughput sequencing reads. *EMBnet J.* **17**, 10-12. doi:10.1089/cmb.2017.0096

Meno, C., Gritsman, K., Ohishi, S., Ohfuji, Y., Heckscher, E., Mochida, K., Shimono, A., Kondoh, H., Talbot, W. S., Robertson, E. J. et al. (1999). Mouse Lefty2 and zebrafish antivin are feedback inhibitors of nodal signaling during vertebrate gastrulation. *Mol. Cell* **4**, 287-298. doi:10.1016/S1097-2765(00)80331-7

Morgani, S. M. and Hadjantonakis, A.-K. (2020). Signaling regulation during gastrulation: Insights from mouse embryos and in vitro systems. *Curr. Top. Dev. Biol.* **137**, 391-431. doi:10.1016/bs.ctdb.2019.11.011

Nowotschin, S., Ferrer-Vaquer, A., Concepcion, D., Papaioannou, V. E. and Hadjantonakis, A.-K. (2012). Interaction of Wnt3a, Msgn1 and Tbx6 in neural versus paraxial mesoderm lineage commitment and paraxial mesoderm differentiation in the mouse embryo. *Dev. Biol.* **367**, 1-14. doi:10.1016/j.ydbio.2012.04.012

Oginuma, M., Hirata, T. and Saga, Y. (2008). Identification of presomitic mesoderm (PSM)-specific Mesp1 enhancer and generation of a PSM-specific Mesp1/Mesp2-null mouse using BAC-based rescue technology. *Mech. Dev.* **125**, 432-440. doi:10.1016/j.mod.2008.01.010

Oh, S., Shao, J., Mitra, J., Xiong, F., D'Antonio, M., Wang, R., Garcia-Bassets, I., Ma, Q., Zhu, X., Lee, J.-H. et al. (2021). Enhancer release and retargeting activates disease-susceptibility genes. *Nature* **595**, 735-740. doi:10.1038/s41586-021-03577-1

Olson, E. N., Arnold, H.-H., Rigby, P. W. J. and Wold, B. J. (1996). Know your neighbors: three phenotypes in null mutants of the myogenic bHLH gene MRF4. *Cell* **85**, 1-4. doi:10.1016/S0092-8674(00)81073-9

Rivera-Perez, J. A. and Magnuson, T. (2005). Primitive streak formation in mice is preceded by localized activation of Brachyury and Wnt3. *Dev. Biol.* **288**, 363-371. doi:10.1016/j.ydbio.2005.09.012

Robertson, E. J. (2014). Dose-dependent Nodal/Smad signals pattern the early mouse embryo. *Semin. Cell Dev. Biol.* **32**, 73-79. doi:10.1016/j.semcdb.2014.03.028

Russ, A. P., Wattler, S., Colledge, W. H., Aparicio, S. A., Carlton, M. B., Pearce, J. J., Barton, S. C., Surani, M. A., Ryan, K., Nehls, M. C. et al. (2000). Eomesodermin is required for mouse trophoblast development and mesoderm formation. *Nature* **404**, 95-99. doi:10.1038/35003601

Sadahiro, T., Isomi, M., Muraoka, N., Kojima, H., Haginiwa, S., Kurotsu, S., Tamura, F., Tani, H., Tohyama, S., Fujita, J. et al. (2018). Tbx6 induces nascent mesoderm from pluripotent stem cells and temporally controls cardiac versus somite lineage diversification. *Cell Stem Cell* **23**, 382-395.e385. doi:10.1016/j.stem.2018.07.001

Saga, Y. (1998). Genetic rescue of segmentation defect in MesP2-deficient mice by MesP1 gene replacement. *Mech. Dev.* **75**, 53-66. doi:10.1016/S0925-4773(98)00077-X

Saga, Y., Yagi, T., Ikawa, Y., Sakakura, T. and Aizawa, S. (1992). Mice develop normally without tenascin. *Genes Dev.* **6**, 1821-1831. doi:10.1101/gad.6.10.1821

Saga, Y., Hata, N., Kobayashi, S., Magnuson, T., Seldin, M. F. and Taketo, M. M. (1996). MesP1: a novel basic helix-loop-helix protein expressed in the nascent mesodermal cells during mouse gastrulation. *Development* **122**, 2769-2778. doi:10.1242/dev.122.9.2769

Saga, Y., Hata, N., Koseki, H. and Taketo, M. M. (1997). Mesp2: a novel mouse gene expressed in the presegmented mesoderm and essential for segmentation initiation. *Genes Dev.* **11**, 1827-1839. doi:10.1101/gad.11.14.1827

Saga, Y., Miyagawa-Tomita, S., Takagi, A., Kitajima, S., Miyazaki, J. and Inoue, T. (1999). MesP1 is expressed in the heart precursor cells and required for the formation of a single heart tube. *Development* **126**, 3437-3447. doi:10.1242/dev.126.15.3437

Saga, Y., Kitajima, S. and Miyagawa-Tomita, S. (2000). Mesp1 expression is the earliest sign of cardiovascular development. *Trends Cardiovasc. Med.* **10**, 345-352. doi:10.1016/S1050-1738(01)00069-X

Saijoh, Y., Adachi, H., Sakuma, R., Yeo, C.-Y., Yashiro, K., Watanabe, M., Hashiguchi, H., Mochida, K., Ohishi, S., Kawabata, M. et al. (2000). Left-right asymmetric expression of lefty2 and nodal is induced by a signaling pathway that includes the transcription factor FAST2. *Mol. Cell* **5**, 35-47. doi:10.1016/S1097-2765(00)80401-3

Sakuma, R., Ohnishi, Y.-I., Meno, C., Fujii, H., Juan, H., Takeuchi, J., Ogura, T., Li, E., Miyazono, K. and Hamada, H. (2002). Inhibition of Nodal signalling by Lefty mediated through interaction with common receptors and efficient diffusion. *Genes Cells* **7**, 401-412. doi:10.1046/j.1365-2443.2002.00528.x

Seidl, K. J., Manis, J. P., Bottaro, A., Zhang, J., Davidson, L., Kisselgof, A., Oettgen, H. and Alt, F. W. (1999). Position-dependent inhibition of class-switch recombination by PGK-neor cassettes inserted into the immunoglobulin heavy chain constant region locus. *Proc. Natl. Acad. Sci. USA* **96**, 3000-3005. doi:10.1073/pnas.96.6.3000

Simon, C. S., Downes, D. J., Gosden, M. E., Telenius, J., Higgs, D. R., Hughes, J. R., Costello, I., Bikoff, E. K. and Robertson, E. J. (2017). Functional characterisation of cis-regulatory elements governing dynamic Eomes expression in the early mouse embryo. *Development* **144**, 1249-1260. doi:10.1242/dev.147322

Takada, S., Stark, K. L., Shea, M. J., Vassileva, G., McMahon, J. A. and McMahon, A. P. (1994). Wnt-3a regulates somite and tailbud formation in the mouse embryo. *Genes Dev.* **8**, 174-189. doi:10.1101/gad.8.2.174

Takahashi, Y., Koizumi, K., Takagi, A., Kitajima, S., Inoue, T., Koseki, H. and Saga, Y. (2000). Mesp2 initiates somite segmentation through the Notch signalling pathway. *Nat. Genet.* **25**, 390-396. doi:10.1038/78062

Takahashi, Y., Kitajima, S., Inoue, T., Kanno, J. and Saga, Y. (2005). Differential contributions of Mesp1 and Mesp2 to the epithelialization and rostro-caudal patterning of somites. *Development* **132**, 787-796. doi:10.1242/dev.01597

Takahashi, Y., Yasuhiko, Y., Kitajima, S., Kanno, J. and Saga, Y. (2007). Appropriate suppression of Notch signaling by Mesp factors is essential for stripe pattern formation leading to segment boundary formation. *Dev. Biol.* **304**, 593-603. doi:10.1016/j.ydbio.2007.01.007

Takemoto, T., Uchikawa, M., Yoshida, M., Bell, D. M., Lovell-Badge, R., Papaioannou, V. E. and Kondoh, H. (2011). Tbx6-dependent Sox2 regulation determines neural or mesodermal fate in axial stem cells. *Nature* **470**, 394-398. doi:10.1038/nature09729

Tam, P. P. L. and Behringer, R. R. (1997). Mouse gastrulation: the formation of a mammalian body plan. *Mech. Dev.* **68**, 3-25. doi:10.1016/S0925-4773(97)00123-8

Tam, P. P. L. and Loebel, D. A. F. (2007). Gene function in mouse embryogenesis: get set for gastrulation. *Nat. Rev. Genet.* **8**, 368-381. doi:10.1038/nrg2084

Tortelote, G. G., Hernández-Hernández, J. M., Quaresma, A. J. C., Nickerson, J. A., Imbalzano, A. N. and Rivera-Pérez, J. A. (2013). Wnt3 function in the epiblast is required for the maintenance but not the initiation of gastrulation in mice. *Dev. Biol.* **374**, 164-173. doi:10.1016/j.ydbio.2012.10.013

Tosic, J., Kim, G.-J., Pavlovic, M., Schröder, C. M., Mersiowsky, S.-L., Barg, M., Hofherr, A., Probst, S., Köttgen, M., Hein, L. et al. (2019). Eomes and Brachyury control pluripotency exit and germ-layer segregation by changing the chromatin state. *Nat. Cell Biol.* **21**, 1518-1531. doi:10.1038/s41556-019-0423-1

van den Ameele, J., Tiberi, L., Bondue, A., Paulissen, C., Herpoel, A., Iacovino, M., Kyba, M., Blanpain, C. and Vanderhaeghen, P. (2012). Eomesodermin induces Mesp1 expression and cardiac differentiation from embryonic stem cells in the absence of Activin. *EMBO Rep.* **13**, 355-362. doi:10.1038/embor.2012.23

Wada, R., Muraoka, N., Inagawa, K., Yamakawa, H., Miyamoto, K., Sadahiro, T., Umei, T., Kaneda, R., Suzuki, T., Kamiya, K. et al. (2013). Induction of human cardiomyocyte-like cells from fibroblasts by defined factors. *Proc. Natl. Acad. Sci. USA* **110**, 12667-12672. doi:10.1073/pnas.1304053110

West, D. B., Engelhard, E. K., Adkisson, M., Nava, A. J., Kirov, J. V., Cipollone, A., Willis, B., Rapp, J., de Jong, P. J. and Lloyd, K. C. (2016). Transcriptome analysis of targeted mouse mutations reveals the topography of local changes in gene expression. *PLoS Genet.* **12**, e1005691. doi:10.1371/journal.pgen.1005691

Xu, C., Liguori, G., Persico, M. G. and Adamson, E. D. (1999). Abrogation of the Cripto gene in mouse leads to failure of postgastrulation morphogenesis and lack of differentiation of cardiomyocytes. *Development* **126**, 483-494. doi:10.1242/dev.126.3.483

Yabe, T., Hoshijima, K., Yamamoto, T. and Takada, S. (2016). Quadruple zebrafish mutant reveals different roles of Mesp genes in somite segmentation between mouse and zebrafish. *Development* **143**, 2842-2852. doi:10.1242/dev.133173

Yamaguchi, T. P., Takada, S., Yoshikawa, Y., Wu, N. and McMahon, A. P. (1999). T (Brachyury) is a direct target of Wnt3a during paraxial mesoderm specification. *Genes Dev.* **13**, 3185-3190. doi:10.1101/gad.13.24.3185

Yasuhiko, Y., Haraguchi, S., Kitajima, S., Takahashi, Y., Kanno, J. and Saga, Y. (2006). Tbx6-mediated Notch signaling controls somite-specific Mesp2 expression. *Proc. Natl. Acad. Sci. USA* **103**, 3651-3656. doi:10.1073/pnas.0508238103

Yasuhiko, Y., Kitajima, S., Takahashi, Y., Oginuma, M., Kagiwada, H., Kanno, J. and Saga, Y. (2008). Functional importance of evolutionally conserved Tbx6 binding sites in the presomitic mesoderm-specific enhancer of Mesp2. *Development* **135**, 3511-3519. doi:10.1242/dev.027144

Yoon, Y., Huang, T., Tortelote, G. G., Wakamiya, M., Hadjantonakis, A.-K., Behringer, R. R. and Rivera-Pérez, J. A. (2015). Extra-embryonic Wnt3 regulates the establishment of the primitive streak in mice. *Dev. Biol.* **403**, 80-88. doi:10.1016/j.ydbio.2015.04.008

Yoshida, T., Vivatbutsiri, P., Morriss-Kay, G., Saga, Y. and Iseki, S. (2008). Cell lineage in mammalian craniofacial mesenchyme. *Mech. Dev.* **125**, 797-808. doi:10.1016/j.mod.2008.06.007

Zhao, J., Li, S., Trilok, S., Tanaka, M., Jokubaitis-Jameson, V., Wang, B., Niwa, H. and Nakayama, N. (2014). Small molecule-directed specification of sclerotome-like chondroprogenitors and induction of a somitic chondrogenesis program from embryonic stem cells. *Development* **141**, 3848-3858. doi:10.1242/dev.105981